

## In Situ Calibration of Underwater Glider Flight Model Using Acoustic Doppler Current Profilers

T. TANAKA,<sup>a</sup> D. HASEGAWA,<sup>a</sup> T. OKUNISHI,<sup>a</sup> I. YASUDA,<sup>b</sup> AND T. P. WELCH<sup>c</sup>

<sup>a</sup>*Fisheries Resources Institute, Japan Fisheries Research and Education Agency, Miyagi, Japan*

<sup>b</sup>*Atmosphere and Ocean Research Institute, The University of Tokyo, Chiba, Japan*

<sup>c</sup>*College of Earth, Ocean, and Atmospheric Sciences, Oregon State University, Corvallis, Oregon*

(Manuscript received 10 June 2021, in final form 26 April 2022)

**ABSTRACT:** The angle of attack (AOA) is the difference between the underwater glider's path and pitch angle and is necessary to accurately estimate dead-reckoned position and depth-averaged velocity. The AOA is also important for any sensor measurements that are affected by the glider's velocity through water, such as ocean turbulence measurement. A glider flight model is generally used to accurately estimate AOA and glider's actual velocity based on the knowledge of lift and drag coefficients optimized for each glider. This paper examines the AOA of a Slocum glider using an acoustic Doppler current profiler (ADCP) to demonstrate a regression method to estimate these coefficients. Since the current shear was sufficiently small on average, it was reasonable to assume that the ADCP velocity at the nearest bin could capture the glider's motion during flight and was used to calculate AOA. The lift and drag coefficients were optimized so the flight model estimated the observed pitch–AOA relationship derived from the ADCP and the glider's pitch observations. The resultant coefficients also satisfied the vertical and horizontal constraints of glider motion and gave unbiased estimates of turbulence intensity derived from the flight model and ADCP. Our method was also applied to a SeaExplorer glider to derive the lift and drag coefficients for the first time. The observed pitch–AOA relationship was reasonably captured by the flight model with the resultant coefficients, suggesting that our method to estimate the lift and drag coefficient of underwater gliders can be applied to any type of underwater glider equipped with an ADCP.

**KEYWORDS:** Ocean; Mixing; Acoustic measurements/effects; In situ oceanic observations; Instrumentation/sensors

### 1. Introduction

Autonomous underwater gliders have been widely used in various aspects of ocean research in recent years (Rudnick 2016) including small-scale turbulence measurements in the ocean interior (Fer et al. 2014; Peterson and Fer 2014; Palmer et al. 2015; Schultze et al. 2017; Scheifele et al. 2018). When the gliders dive or climb by controlling their buoyancy, the lift force exerted on the underwater gliders produces forward motion, and thus the glider's flight becomes sawtooth paths. The glider's path angle consists of the pitch angle  $\theta$ , which is normally monitored by the navigational sensors of the glider, and the angle of attack  $\alpha$ , which is nonzero during the flight [ $\gamma = \theta + \alpha$ , henceforth AOA (Fig. 1a)]. The accurate estimate of AOA is important for all of the gliders in terms of both the scientific and navigational purposes, as the calculation of dead-reckoned position and thus the depth-average velocity relies on the accuracy of AOA estimation [e.g., Rudnick et al. (2018) for Spray glider; Bennett et al. (2021) for Seaglider]. Knowledge of glider's flight is also important for sensor measurements of any ocean variables that are affected by the glider's speed through water ( $v_g$  in Fig. 1a); in particular, turbulence energy dissipation rate, which is often measured by

airfoil shear probes (Osborn 1974), is proportional to  $v_g^{-4}$  (Lueck et al. 1997).

The steady-state flight model proposed by Merckelbach et al. (2010, henceforth MEA10), which assumes a dynamical force balance exerted on the glider, has been widely used to estimate the AOA and the glider's speed through water for Slocum gliders (Teledyne Webb Research, North Falmouth, Massachusetts). As described in section 2a, the flight model gives AOA as

$$\alpha = \frac{C_{D0} + C_{D1}\alpha^2}{(a_h + a_w)\tan(\theta + \alpha)}, \quad (1)$$

where  $a_h$  and  $a_w$  are the lift coefficients for the hull and wings, respectively, and  $C_{D0}$  and  $C_{D1}$  are the drag coefficients due to parasite and induced drag, respectively (MEA10). Thus, if the knowledge of lift and drag coefficients is available, AOA can be estimated solely from the pitch angle monitored by the glider for the steady state. The information of AOA as well as these coefficients is also required for the flight model to estimate  $v_g$  [Eq. (8) as mentioned in section 2a].

Continuing efforts on the estimation of the lift and drag coefficients have been made for Slocum gliders (e.g., Williams et al. 2008; Cooney 2011). Based on the predetermined  $a_h$ ,  $a_w$ , and  $C_{D1}$  derived from laboratory experiments and semiempirical formula, MEA10 proposed a method to calibrate  $C_{D0}$  so that the modeled vertical speed matched the measured pressure/depth rate (see section 2a for details). Merckelbach et al. (2019, henceforth MEA19) also used the axial speed of

<sup>a</sup> Denotes content that is immediately available upon publication as open access.

Corresponding author: Takahiro Tanaka, takahiro@affrc.go.jp

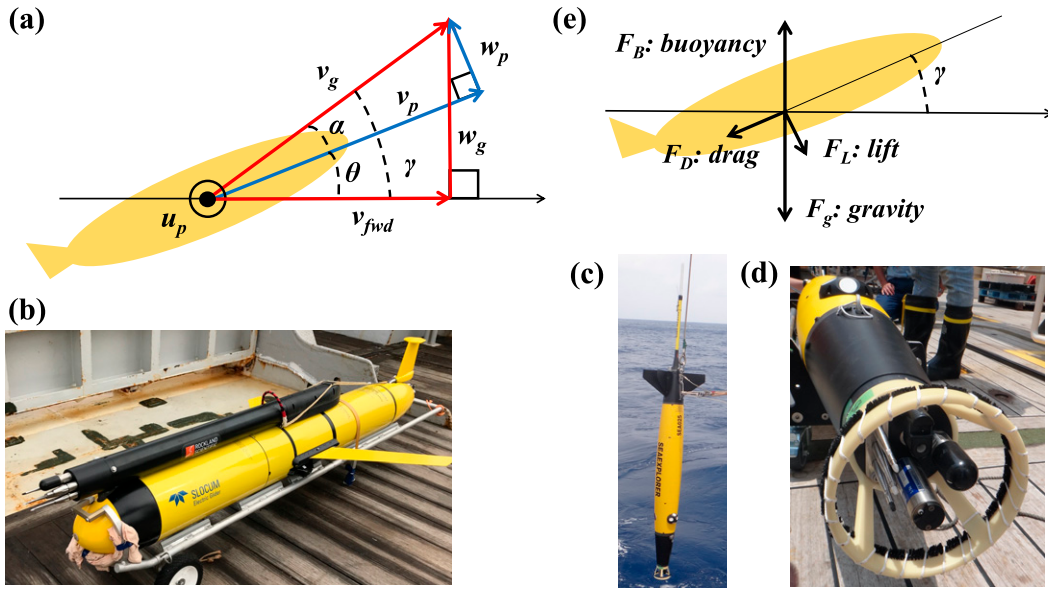


FIG. 1. (a) Configuration of the velocities and angles referred in the text and the following figures. The positive direction of  $u_p$  is out of the page. (e) Schematic of the forces exerted on the glider body. Pictures of (b) the Slocum G2 glider (unit 095) and (c) the SeaExplorer (SEA025) used in this study. (d) The SeaExplorer had a sensor guard at the front of the microstructure profiler.

the glider measured by an acoustic Doppler current profiler (hereafter ADCP) or an electromagnetic current sensor (hereafter EM sensor) to estimate the total lift coefficient  $a (=a_h + a_w)$  by matching the modeled and measured horizontal glider motion (see section 4b for the method). Although efforts to construct the flight model have also been made for other types of gliders, such as Seagliders (e.g., Frajka-Williams et al. 2011) and Sprays (e.g., Sherman et al. 2001), the knowledge of the flight model is often limited, especially for gliders recently released to the oceanographic community (such as the SeaExplorer gliders, Alseamar, France). This lack of knowledge makes it difficult to estimate AOA and thus the glider speed through water for these gliders.

Instead of using the flight model, Todd et al. (2017, henceforth TEA17) estimated AOA from velocity measurements made by an ADCP installed on their Spray gliders (see section 2b for their method). The purpose of this study is to demonstrate a regression method to estimate the lift and drag coefficients of the flight model based on the knowledge of AOA derived from the ADCP measurements (section 3). This study uses data from Slocum (Fig. 1b) and SeaExplorer (Figs. 1c,d) glider deployments in 2017, all of which have ADCPs installed (see section 2b and 2c for the mission details). By applying our method to the SeaExplorer glider data, this study also aims to estimate the lift and drag coefficients of the SeaExplorer for the first time (see section 3b). After the validity and technical limitation of our method is discussed in section 4a, our resultant AOA is compared with that derived from the coefficients estimated by the methods of MEA10 and MEA19 (section 4b), showing that they agree with each other within a factor of 5%. Since our

gliders also have an EM sensor which measures the axial speed of the glider ( $v_p$  in Fig. 1a), a method to estimate lift and drag coefficients from the EM sensor data is discussed in appendix E.

## 2. Data and method

### a. Steady-state flight model

This subsection describes the method to optimize the parasite drag coefficients  $C_{D0}$  of the steady-state flight model made by MEA10 using the measured pressure/depth rate as a vertical constraint of the glider motion. They assumed a quasi-steady force balance (Fig. 1e):

$$\text{Vertical : } F_B - F_g - \cos\gamma F_L - \sin\gamma F_D = 0, \quad (2)$$

$$\text{Horizontal : } \sin\gamma F_L - \cos\gamma F_D = 0, \quad (3)$$

where  $F_B$  is the buoyancy force,  $F_g$  the gravitational force,  $F_L$  the lift force, and  $F_D$  the drag force. Since  $F_L$  and  $F_D$  can be written as

$$F_L = 1/2 \times \rho C_L S v_g^2, \quad (4)$$

$$F_D = 1/2 \times \rho C_D S v_g^2, \quad (5)$$

where the lift and drag coefficients,  $C_L$  and  $C_D$ , respectively, are parameterized as

$$C_L = (a_h + a_w)\alpha, \quad (6)$$

$$C_D = C_{D0} + C_{D1}\alpha^2, \quad (7)$$

the horizontal force balance [Eq. (3)] gives the AOA as Eq. (1). In these equations,  $\rho$  is the seawater density, and  $S$  the surface area of wings. For computational efficiency, this study solved Eq. (1) by doing a Taylor series expansion of sine and cosine about  $\theta$  to make a cubic equation in  $\alpha$  (see [appendix A](#) for details).

To determine  $C_{D0}$ ,  $v_g$  was derived from the vertical force balance [Eq. (2)] as

$$v_g^2 = \frac{2 \sin \gamma}{\rho (C_{D0} + C_{D1} \alpha^2) S} (F_B - F_g); \quad (8)$$

$F_B$  and  $F_g$  can be written as

$$F_B = \rho g \{V_{GL}[1 - cP + \beta(T - T_0)] + V_{oil}\}, \quad (9)$$

$$F_g = mg, \quad (10)$$

where  $g$  is the gravitational acceleration ( $=9.80 \text{ m s}^{-2}$  in this study),  $V_{GL}$  the volume of the glider,  $c$  the compressibility of the glider body,  $P$  the water pressure,  $\beta$  the thermal expansion coefficient,  $T$  the water temperature,  $T_0$  the reference water temperature,  $V_{oil}$  the hydraulic oil volume outside the glider, and  $m$  the total mass of the glider. In this study,  $\beta$  was set to zero since the result was not significantly affected even if a more realistic value (for instance,  $53.5 \times 10^{-6} \text{ }^{\circ}\text{C}^{-1}$  given by the manufacturer of the Slocum glider; [Teledyne Webb Research 2012](#)<sup>1</sup>) was used. If the knowledge of  $a_h$ ,  $a_w$ , and  $C_{D1}$  is available,  $C_{D0}$ ,  $c$ , and  $V_{GL}$  were determined by minimizing the difference between the estimated vertical fall rate from the pressure/depth sensor (i.e.,  $w_g = dP/dt$ , where  $d/dt$  denotes the time derivative) and computed by the flight model (i.e.,  $v_g \sin \gamma$ ). The cost function in this study was

$$CF = \sum (w_g - v_g \sin \gamma)^2, \quad (11)$$

where the summation is over all the data points of each glider. Since the measured  $w_g$  is positive during descent, while the pitch angle is negative, the sign of  $w_g$  is reversed in Eq. (11). Hereafter, this optimization procedure to obtain  $C_{D0}$ ,  $c$ , and  $V_{GL}$  is referred to as the [MEA10](#) method.

### b. Slocum glider mission

#### 1) INSTRUMENTS AND DATA COLLECTION

A glider mission was conducted in 2017 from 24 until 31 July across the Oyashio, east of Japan (blue dots in [Fig. 2a](#)) using a Slocum G2 glider (unit 095, 1000 m depth rating, and a mass,  $m$ , of 70.0 kg in this study). The depth, pitch, roll, heading, battery position, and oil volume of the glider were recorded by the navigation board at a frequency of 0.25 Hz. The glider had an unpumped CTD (Neil Brown Ocean Sensors, Inc.; [Schmitt and Petitt 2006](#)), whose sampling rate was 1 Hz.

<sup>1</sup> The thermal expansion coefficient in this manual (i.e.,  $535 \times 10^{-6} \text{ }^{\circ}\text{C}^{-1}$ ) is a typo, and the correct value is  $53.5 \times 10^{-6} \text{ }^{\circ}\text{C}^{-1}$  according to the manufacturer ([Teledyne Webb Research 2021](#), personal communication).

The microstructure profiler [Microrider from Rockland Scientific Inc. (henceforth MR)] was mounted on top ([Fig. 1b](#)) and had an EM sensor (JFE Advantec Co., Ltd., AEM1-GA), which measured  $v_p$  at 64 Hz. In addition to the MR, a 4-beam phased-array ADCP (Teledyne RDI, DVL Explorer, 600 kHz) was mounted on the bottom, and the transducer was installed with a pitch angle of  $11^{\circ}$  forward so that the orientation of three beams was designed to be  $15^{\circ}$  from vertical when the glider dives with a nominal pitch angle of  $26^{\circ}$ . The ADCP velocity data were recorded every 3–4 s in Earth coordinates. There are 30 bins with a bin size of 2 m each, and the nearest bin was 2.9 m from the transducer. The recording of the ADCP was done only for the descent during this mission. The depth transducer, pitch, roll, and heading were also recorded in the ADCP data at the same interval. Since the ADCP did not have independent compass, pressure, or tilt sensors, these data were taken from the navigation board. We note that the offset of pitch and roll angle was estimated as  $-0.5^{\circ}$  and  $5.6^{\circ}$ , respectively, so that the vertical velocity  $w_g$  derived from the ADCP and the pressure sensor, matched (see [appendix B](#) for details). We also note that the depth/pressure values from the navigation/CTD sensors were contaminated by high frequency noise as similarly mentioned by [MEA10](#). Thus,  $w_g$  derived from these sensors was moving averaged over 60 s in this study.

#### 2) DATA PROCESSING

The 1 Hz CTD time series were averaged into a 0.25 Hz time series after correcting temperature and conductivity mismatch following [Garau et al. \(2011\)](#). Then all variables derived from the navigation, MR, and ADCP sensors were linearly interpolated to the 0.25 Hz CTD time series after adjusting the time offset of the MR and ADCP as described in the following. The time offset of the MR was adjusted so that the time of reaching maximum depth derived from the CTD and the MR matched for each cast. The lag of the MR clock was less than 5 s during the mission. After adjusting the offset, the MR data were first moving averaged over 4 s before being linearly interpolated to the 0.25 Hz CTD time series.

The time offset of the ADCP was adjusted so that the pitch from navigation and ADCP sensors matched for each cast. The ADCP lagged navigation by about 9 s throughout the entire mission. The ADCP data obtained from the nearest bin were used for analysis, as the influence of current shear between the depth of glider and the depth of velocity measurement is expected to be minimized, which is assessed in [section 3a](#). The nearest bin was also away from the boundary layer, which is typically less than 0.1 m ([TEA17](#)). We note that although the velocity data obtained from deeper bins are considered to have a larger influence from current shear, the resultant lift and drag coefficients, as well as AOA, did not change significantly by more than a factor of 5% from those shown in [section 3a](#) among bin1–bin4 (see [appendix C](#) for details).

The initial data quality control was done following [TEA17](#) and passed if all the requirements below were satisfied:

- R1) the velocity was  $0.5 \text{ m s}^{-1}$  or less,
- R2) the echo intensity (or amplitude) was 75 dB or less,

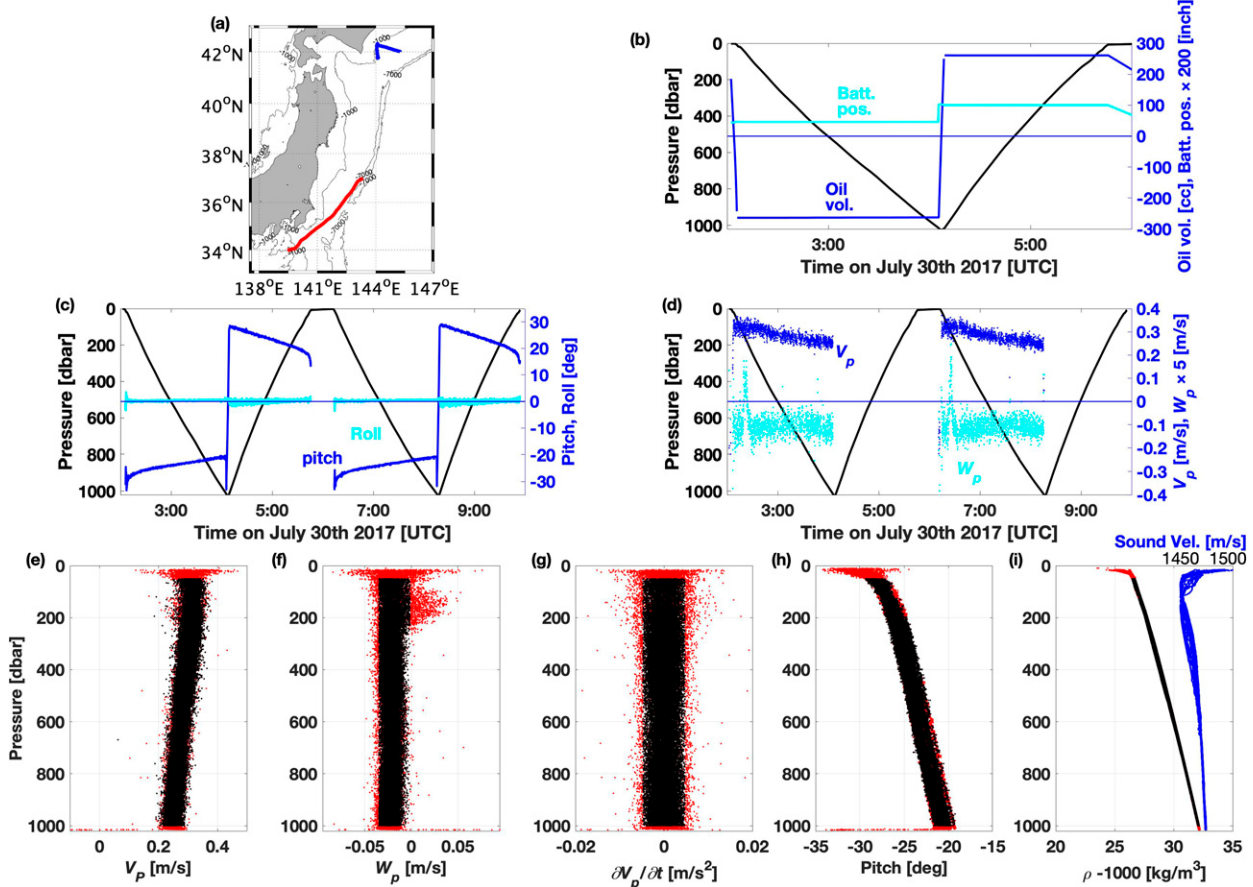


FIG. 2. (a) Surface locations of the Slocum (blue line) and SeaExplorer (red line) glider deployments. Contours are 1000, 4000, and 7000 m isobaths. (b) Time series of pressure (black), oil volume (blue), and battery position (cyan) for the Slocum mission on 30 Jul 2017. (c) As in (b), but for pitch (blue) and roll (cyan). (d) As in (b), but for the along-glider velocity  $v_p$  (blue) and vertical-glider velocity  $w_p$  (cyan). Note that the battery position in (c) and  $w_p$  in (d) are multiplied by 200 and 5, respectively, to fit the scale. Also shown are the vertical profiles of (e) along-glider velocity  $v_p$ , (f) vertical-glider velocity  $w_p$ , (g) along-glider acceleration,  $\partial v_p / \partial t$ , (h) pitch angle  $\theta$ , and (i) in situ seawater density  $\rho$  (black), and sound velocity (blue) for the descent casts of the Slocum mission. (e)–(g) are derived from the ADCP sensor. Black (red) dots are the data used (excluded) from the analysis based on the selection criteria listed in Table 1.

- R3) the percent good was 80% or greater, and
- R4) the signal-to-noise ratio (SNR) was 20 or greater.

In this study, a scale factor of 0.45 (Deines 1999) was applied to convert the raw RSSI counts to dB, and the percent good was defined as the sum of good 3- and 4-beam solutions. SNR was defined as  $\text{SNR} = 10^{(\text{Sig-Noise})/10}$ , where “Sig” and “Noise” was the echo intensity and the noise level, both in dB. The noise level was set to be 26.5 dB, determined from the echo intensity of the farthest bin (appendix C).

To estimate AOA using the ADCP data of the nearest bin, the velocity data were expressed in glider coordinates using the heading  $\varphi$ , pitch  $\theta$ , and roll  $\zeta$ . The axis orientation is a right-hand coordinate system, where the along-glider axis is from the rear to the front of the glider, the cross-glider axis is from the port to the starboard, and the vertical-glider axis is perpendicular to the along-glider and positive upward in this study (Fig. 1a). Since AOA is defined in the vertical plane between the glider’s forward and downward motion (TEA17), the

cross-, along-, and vertical-glider velocities denoted by  $u_p$ ,  $v_p$ , and  $w_p$ , respectively (Fig. 1a), were calculated as

$$u_p = v \sin \varphi - u \cos \varphi, \quad (12)$$

$$v_p = -(u \sin \varphi + v \cos \varphi) \cos \theta - w \sin \theta, \quad (13)$$

$$w_p = (u \sin \varphi + v \cos \varphi) \sin \theta - w \cos \theta, \quad (14)$$

where  $u$ ,  $v$ , and  $w$  are eastward, northward, and vertical velocities, respectively, recorded by the ADCP. This coordinate transform enables us to estimate AOA from the geometry in Fig. 1a by

$$\alpha = \arctan \left( \frac{w_p}{v_p} \right). \quad (15)$$

After the coordinate transformation from the Earth coordinates to the glider coordinates through Eqs. (12)–(14) and correcting

TABLE 1. The list of minimum and maximum thresholds for the data selection criteria of each variable for the Slocum. The mean and standard deviation (std) after screening the data are also listed for the descent. A long dash denotes that no threshold was set. Note that 1 in. = 25.4 mm.

	Min/max	Mean (std)
Pressure ( $P$ , dbar)	50/1000	534.6 (272.1)
Pitch ( $\theta$ , °)	—/—	-23.69 (1.97)
Roll ( $\zeta$ , °)	—/—	0.11 (0.26)
Oil volume ( $V_{\text{oil}}$ , mL)	—/-250	-263.1 (0.85)
Battery position (in.)	—/—	0.22 (0.014)
Vertical fall rate ( $w_g$ , m s <sup>-1</sup> )	0.05/—	0.13 (0.019)
Vertical acceleration ( $\partial w_g / \partial t$ , m s <sup>-2</sup> )	—/—	$-8.65 \times 10^{-6}$ ( $5.15 \times 10^{-5}$ )
Along-glider velocity ( $v_p$ , m s <sup>-1</sup> )	—/—	0.28 (0.027)
Along-glider acceleration ( $\partial v_p / \partial t$ , m s <sup>-2</sup> )	-0.0048/0.0048	$-1.61 \times 10^{-5}$ (0.0020)
Vertical-glider velocity ( $w_p$ , m s <sup>-1</sup> )	-0.0348/-0.0010	-0.021 (0.0061)
Cross-glider velocity ( $u_p$ , m s <sup>-1</sup> )	—/—	0.0009 (0.015)

the roll offset [using Eqs. (B6) and (B7) in appendix B], the data were linearly interpolated to the 0.25 Hz CTD time series and then were corrected based on the sound speed determined from the CTD data. It is also noted that TEA17 computed AOA by  $\alpha = \arctan(w/v_{\text{fwd}}) - \theta$ , where  $v_{\text{fwd}}$  is the glider's forward speed in the horizontal plane (Fig. 1a), similarly derived from the coordinate transform. Using Eq. (15), their formula can be derived mathematically.

We analyzed all the casts reaching 1000 m depth when both the MR and ADCP data were available. For the first few casts after deployment, some short dives to about 500 m depth were made using the servo control to adjust the glider's pitch angle to a nominal value of  $\pm 26^\circ$ . Then 1000 m dives were started with the battery position fixed at a position for stable flight to avoid vibration due to battery motion (Fig. 2b). Figures 2b–d are the typical time series of the navigational and ADCP data, and Figs. 2e–i are the vertical profiles of all the descent casts based on the ADCP, navigation, and CTD data. The mean and standard deviation of each variable is listed in Table 1.

The ascent speed was generally faster than the descent since the glider was ballasted light for the water density in our observational site with full buoyancy displacement. The magnitude of pitch angle decreased as the glider went deeper during descent due to the pressure compressibility and thermal expansion/contraction of the hull shifting the center of buoyancy (Figs. 2c,h). The roll angle was almost constant at  $0.1^\circ$  during descent, while the roll fluctuated more during ascent (Fig. 2c). The oil volume of the glider was fully pumped to the internal reservoir during descent ( $-260$  mL, Fig. 2b).

Since the ADCP did not record during ascent, only descent data were used for analysis. Typically,  $v_p$  derived from the ADCP decreased from about  $0.30$  m s<sup>-1</sup> near the sea surface to  $0.25$  m s<sup>-1</sup> near the bottom (Figs. 2d,e). The glider motion and attitude variance were larger near the sea surface and at the turning depth when the oil bladder was inflated ( $P > 1000$  dbar) (Figs. 2e–h). The vertical-glider velocity,  $w_p$ , did not have an obvious depth dependency, but large fluctuations were

occasionally found at about 150–200 m depth where  $w_p$  became positive (Figs. 2d,f). This depth range was below the pycnocline (Fig. 2i), where a large change of pitch was observed (Fig. 2h). This depth range also corresponded to the sound speed minimum layer due to the influence of the subsurface cold Oyashio water (Fig. 2i) forming a sound channel where sound waves can travel a long distance from the source. The depth of sound speed minimum in the subarctic western North Pacific is much shallower than the typical depth of 1000 m in the ocean (Munk and Forbes 1989). Although the influence of sound channel on the acoustic measurement of water velocity should be further examined in the future, the positive  $w_p$  during descent is dynamically unreasonable because that would result in positive AOA, and thus the direction of  $F_L$  would be backward [from Eqs. (4) and (6)]. Therefore, after extracting the descent data by  $V_{\text{oil}} < -250$  mL,  $\theta < 0^\circ$ , and  $w_g > 0$  m s<sup>-1</sup>, the data points where all of the following criteria were met were analyzed to ensure the quasi-steady state and remove positive  $w_p$ :

- C1)  $P \geq 50$  dbar and  $P \leq 1000$  dbar,
- C2)  $w_p \geq w_{p,0.025}$  and  $w_p \leq w_{p,0.975}$ ,
- C3)  $w_g \geq 0.05$  m s<sup>-1</sup>, and
- C4)  $\partial v_p / \partial t \geq \partial v_p / \partial t_{0.025}$  and  $\partial v_p / \partial t \leq \partial v_p / \partial t_{0.975}$ ,

where  $X_{0.025}$  and  $X_{0.975}$  denote the 0.025 and 0.975 quantiles of  $X$ , respectively. They are listed in Table 1.

### c. SeaExplorer glider mission

#### 1) INSTRUMENTS AND DATA COLLECTION

Another glider mission was conducted in 2017 from 20 until 26 June along the Kuroshio southeast coast of Japan (red dots in Fig. 2a) using a SeaExplorer glider (SEA025, 700 m depth rating,  $m = 63.45$  kg in this study, Figs. 1c,d). The SeaExplorer has three actuators to control attitude and course during flight: the ballast controls the buoyancy and thus the speed through water of the glider by adjusting the oil volume (between  $-500$  mL, fully inside, and  $500$  mL, fully outside), the linear actuator controls the pitch angle by shifting the battery pack back and forth (between 0 mm, fully backward, and 100 mm,

fully forward), and the angular actuator controls the roll angle and heading by shifting the battery pack port or starboard (nominally between  $-45^\circ$  and  $45^\circ$ , port to the starboard). While the values for the ballast and linear actuator remain unchanged during flight once they are assigned by pilots before diving, the angular actuator is controlled by the glider's navigation system and moves frequently. The navigational sensors collected data for depth, attitude, heading, and the positions of actuators every 20 s.

The MR was installed at the front of the glider with the EM sensor and sensor guard (Fig. 1d). The MR recorded  $v_p$  at 64 Hz. The MR also had a CT sensor (JFE Advantec Co., Ltd.), and temperature and conductivity data were recorded at 64 Hz as well. In addition, a four-beam ADCP (Nortek AD2CP, 1 MHz) was mounted on the top (Figs. 1c,d) and emitted sound waves upward during the flight. The velocity data were recorded every 10 s for both descent and ascent in beam coordinates. The beams from the front and rear transducers are tilted at  $47.5^\circ$ , so the front (rear) beams were designed to be  $25^\circ$  from vertical when the glider climbs (dives) with a nominal pitch angle of  $22.5^\circ$ . There are 30 bins with a bin size of 1 m each, and the nearest bin was 1.2 m from the transducer. The ADCP also measured the pressure, pitch, roll, and heading independently from the navigation sensors and recorded them along with the velocity data at the same interval. The offset of pitch and roll angle was estimated as  $0.6^\circ$  and  $3.0^\circ$ , respectively, so that the  $w_g$  derived from the ADCP and the pressure sensor matched (see appendix B).

## 2) DATA PROCESSING

The data were processed in a similar way to the Slocum data: all variables derived from the navigation and ADCP sensors were linearly interpolated to the 0.1 Hz averaged MR time series after adjusting the time offset. The time offset was adjusted so that the time of reaching maximum depth derived from MR and navigation/ADCP matched for each cast. The navigation and ADCP clocks were about 3 s behind and 9 s ahead of the MR clock, respectively. For the CT sensors attached to the MR, TC mismatch was corrected by a routine provided by the manufacturer [the salinity\_JAC.m code in ODAS MATLAB Library (version 4.4) from Rockland Scientific Inc.]. The default parameters for the lag ( $=0.0234$  s) and for the cutoff frequency of a single-pole low-pass filter ( $=0.73$  Hz) was used to correct the conductivity data.

The ADCP velocity data of the nearest bin were also analyzed, as the influence of current shear on the estimation of glider's speed is expected to be minimized (see section 3b). Since the percent good is not available for the Nortek ADCP, the correlation data were used for the initial quality control instead (TEA17): R5) the correlation was 50 or greater, and R1, R2, R4, and R5 are the criteria for passing the initial quality control. The noise level of the ADCP was set to be 25 dB, also determined from the amplitude of the farthest bin.

The transform from the beam coordinates to the glider coordinates was done by transition matrices designed for

the upward-looking ADCP that were given by the manufacturer (by courtesy of Dr. Orens de Fommervault):

$$\begin{pmatrix} v_p \\ u'_p \\ w'_p \end{pmatrix} = \begin{pmatrix} -1.3563 \operatorname{sgn}(\theta) & 0.5055 \operatorname{sgn}(\theta) & 0.5055 \operatorname{sgn}(\theta) \\ 0 & -1.1831 & 1.1831 \\ 0 & 0.5517 & 0.5517 \end{pmatrix} \begin{pmatrix} v_1 \text{ or } v_3 \\ v_2 \\ v_4 \end{pmatrix}, \quad (16)$$

where  $v_1$ ,  $v_2$ ,  $v_3$ , and  $v_4$  are velocities measured by each beam, and  $v_1$  ( $v_3$ ) is used for descent (ascent). Beams 1, 2, 3, and 4 were derived from front, starboard, rear, and port transducers, respectively. Using the corrected roll angle, the coordinate transform from the beam to the glider coordinates was done by

$$u_p = -u'_p \cos\zeta - w'_p \sin\zeta, \quad (17)$$

$$w_p = u'_p \sin\zeta - w'_p \cos\zeta. \quad (18)$$

The velocity data were linearly interpolated to the 0.1 Hz MR time series and were corrected based on the sound speed derived from temperature and salinity of the MR data. Finally, AOA was calculated by the same way for the Slocum [Eq. (15)].

The typical time series of navigational data are presented in Fig. 3a, and Figs. 3b–g are the vertical profiles of all the descent casts based on the ADCP, navigation, and CT sensor data. The mean and standard deviation of navigational and ADCP data are listed in Table 2. We note that the offset of pitch and roll angle measured by navigation sensor was also determined by the same method we used for the ADCP tilt sensor (see appendix B). The resultant offset was  $0.6^\circ$  and  $4.0^\circ$  for pitch and roll, respectively.

All the descent and ascent casts reaching 700 m depth were analyzed after the oil volume was finally set to be  $-500$  and  $260$  mL for descent and ascent, respectively, to achieve the nominal vertical speed to be  $0.15$ – $0.20$  m s $^{-1}$ . The axial speed and the magnitude of pitch angle were decreased as the glider went deeper during descent as similarly observed in the Slocum mission (Figs. 3a,b,f). Also, the glider motion and pitch angle fluctuated largely near the sea surface (Fig. 3b–d,f). During this mission, the shallow pycnocline was not as evident as that in the Oyashio (Fig. 3g), and the depth of the sound speed minimum layer was situated below 700 m (Fig. 3h).

Since the angular actuator moved port and starboard during the flight (Figs. 3a,e), the roll angle fluctuated more than that for the Slocum (Fig. 3a). The mean roll angle was  $1.9^\circ$  for descent and  $-0.3^\circ$  for ascent, but the roll occasionally fluctuated largely and seemed to affect the stability of the pitch (for instance at 1600 UTC in Fig. 3a). Therefore, the data points with large movement of the angular actuator were also discarded. For the SeaExplorer, after extracting the descent data by  $V_{\text{oil}} < -450$  mL,  $\theta < 0^\circ$ , and  $w_g > 0$  m s $^{-1}$  (ascent data by  $V_{\text{oil}} > 250$  mL,  $\theta > 0^\circ$ , and  $w_g < 0$  m s $^{-1}$ ), the data points satisfying all of C2 and C3 criteria and the following conditions were analyzed to ensure quasi-steady state:

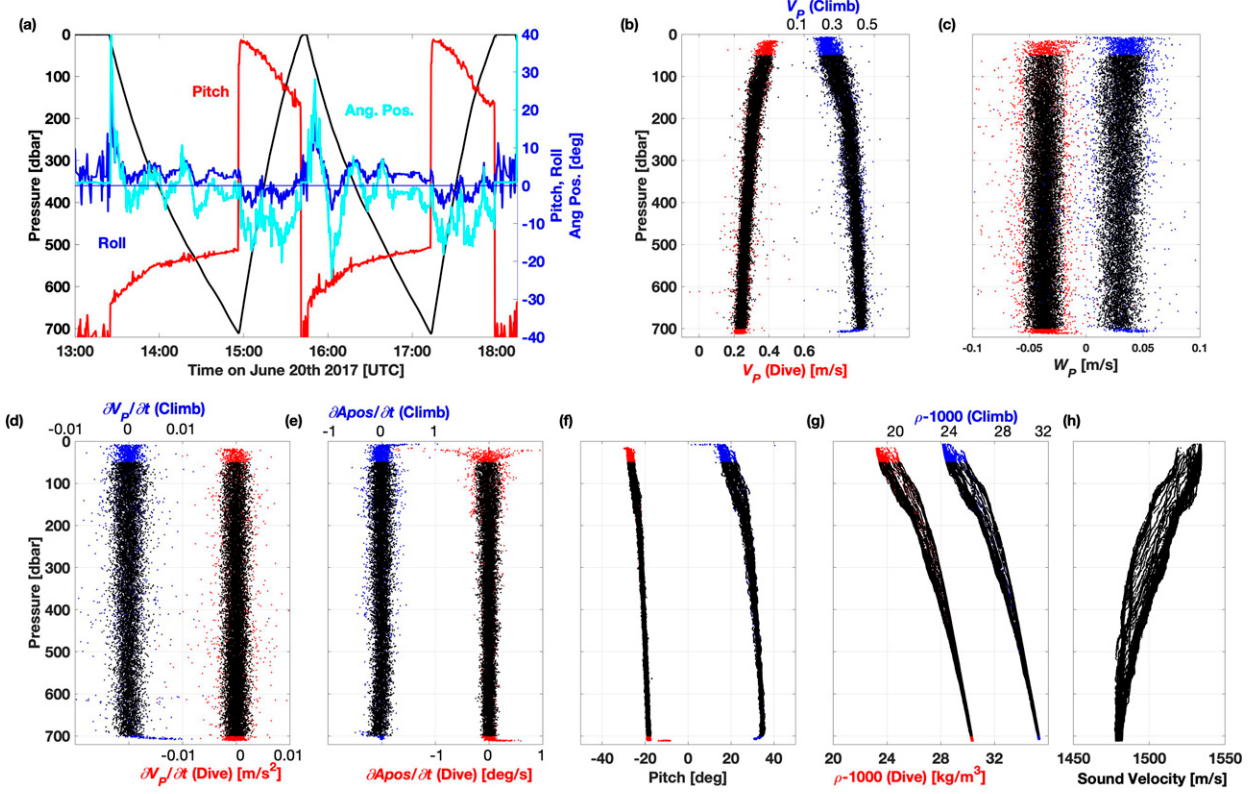


FIG. 3. (a) Time series of pressure (black), pitch (red), roll (blue), and the position of angular actuator position (cyan) for the SeaExplorer mission on 20 Jun 2017. Also shown are the vertical profiles of (b) along-glider velocity  $v_p$ , (c) vertical-glider velocity  $w_p$ , (d) along-glider acceleration  $\partial v_p / \partial t$ , (e) angular actuator motion  $\partial \text{Ang} / \partial t$ , (f) pitch angle  $\theta$ , (g) in situ seawater density  $\rho$ , and (h) sound velocity for both the descent and ascent casts of the SeaExplorer mission. Plots in (b)–(d) are derived from the ADCP sensor. Note that (b), (d), (e), and (g) have a scale on the top of each panel for ascent. Red and blue dots are the data excluded from the analysis for descent and ascent, respectively, based on the selection criteria listed in Table 2. Black dots are used for analysis.

C5)  $P \geq 50$  dbar and  $P \leq 700$  dbar,

C6)  $\partial v_p / \partial t \geq \partial v_p / \partial t_{0.01}$  and  $\partial v_p / \partial t \leq \partial v_p / \partial t_{0.99}$ , and

C7)  $\partial \text{Ang} / \partial t \geq \partial \text{Ang} / \partial t_{0.01}$  and  $\partial \text{Ang} / \partial t \leq \partial \text{Ang} / \partial t_{0.99}$ ,

where “Ang” denotes the position of angular actuator. The data points with negative  $v_p$  were also removed from analysis. The thresholds were separately set for descent and ascent and are listed in Table 2.

### 3. Results

#### a. A method to estimate lift and drag coefficients of the Slocum glider from AOA<sub>ADCP</sub>

After processing and screening data as described in section 2b(2), the mean descending speed derived from the ADCP,  $w_g$ <sub>ADCP</sub> (see appendix B for details of the calculation), was  $0.13 \text{ m s}^{-1}$  for the Slocum glider (Table 1). Since the velocity recorded by the ADCP consists of (i) the glider speed through water, (ii) water velocity at the depth of the glider, and (iii) water velocity at the depth of each bin, the ADCP velocity data would capture the glider speed well if the velocity difference (or the current shear) between (ii) and (iii) is much

smaller than the measured velocity. The mean velocity difference between the first and second nearest bins was  $-9 \times 10^{-4}$  and  $-8 \times 10^{-4} \text{ m s}^{-1}$  for  $v_p$  and  $w_p$ , respectively, and the histogram was well fit by a Gaussian distribution (Figs. 4a,b). Since these values were sufficiently smaller than the mean  $v_p$  and  $w_p$  ( $0.28$  and  $-0.021 \text{ m s}^{-1}$ , respectively, from Table 1), it is reasonable to assume that the current shear does not affect the estimation of the glider’s speed through water significantly if we consider the average values. The mean cross-glider velocity  $u_p$  was about 1% of the mean  $v_p$  (Table 1), and the histogram was well fit by a Gaussian distribution (Fig. 4c). These analyses indicate that the ADCP reasonably captured the glider’s motion through water. During this mission, the mean AOA calculated by Eq. (15) was  $-4.4^\circ$ , and the histogram was also well fit by a Gaussian distribution (Fig. 4d). Since the AOA derived from the flight model is dependent on the pitch angle [Eq. (1)], the following describes a method to obtain the lift and drag coefficients that best explain the observed relationship between the AOA and pitch angle based on the ADCP data (green dots in Fig. 4f).

First,  $c$  and  $V_{\text{GL}}$ , required to calculate  $F_B$  [Eq. (9)], were estimated by the MEA10 method. Using the same values of

TABLE 2. The list of minimum and maximum thresholds for the data selection criteria of each variable for the SeaExplorer. The mean and standard deviation (std) after screening the data is also listed for the descent. A long dash denotes that no threshold was set.

	Descent		Ascent	
	Min/max	Mean (std)	Min/max	Mean (std)
Pressure ( $P$ , dbar)	50/700	407.90 (181.9)	50/700	337.46 (191.4)
Pitch ( $\theta$ , °)	—/—	-20.82 (2.13)	—/—	28.76 (4.87)
Roll ( $\zeta$ , °)	—/—	1.85 (2.81)	—/—	-0.26 (1.80)
Oil volume ( $V_{\text{oil}}$ , mL)	—/-450	-498.5 (1.3)	250/—	259.0 (1.5)
Battery position (mm)	—/—	64.96 (0.20)	—/—	46.09 (0.12)
Angular actuator motion ( $\partial \text{Ang}/\partial t$ , ° s $^{-1}$ )	-0.258/0.242	-0.0013 (0.068)	-0.254/0.271	-0.0026 (0.088)
Vertical fall rate ( $w_g$ , m s $^{-1}$ )	0.05/—	0.14 (0.02)	—/-0.05	-0.21 (0.05)
Vertical acceleration ( $\partial w_g/\partial t$ , m s $^{-2}$ )	—/—	$-1.85 \times 10^{-5}$ ( $1.96 \times 10^{-4}$ )	—/—	$4.30 \times 10^{-5}$ ( $2.65 \times 10^{-4}$ )
Along-glider velocity ( $v_p$ , m s $^{-1}$ )	—/—	0.28 (0.038)	—/—	0.36 (0.055)
Along-glider acceleration ( $\partial v_p/\partial t$ , m s $^{-2}$ )	-0.0031/0.0031	$-2.6 \times 10^{-5}$ (0.0011)	-0.0042/0.0049	$-3.1 \times 10^{-5}$ (0.0014)
Vertical-glider velocity ( $w_p$ , m s $^{-1}$ )	-0.0553/-0.0195	-0.037 (0.0071)	0.0085/0.0527	0.031 (0.0088)
Cross-glider velocity ( $u_p$ , m s $^{-1}$ )	—/—	0.0019 (0.017)	—/—	-0.0044 (0.020)

$C_{D1}$ ,  $a_h$ , and  $a_w$  as in MEA10 (i.e.,  $C_{D1} = 2.88$  rad $^{-2}$ ,  $a_h = 2.4$  rad $^{-1}$ , and  $a_w = 3.7$  rad $^{-1}$ ),  $c$  and  $V_{\text{GL}}$  were  $4.5 \times 10^{-10}$  Pa $^{-1}$  and 68.2 L, respectively. Next, the optimum drag coefficients were estimated by fitting a quadratic function [Eq. (7)] to the observed relationship between the AOA and total drag coefficient,  $C_D$ . According to the flight model [Eqs. (2), (3), and (5)],  $C_D$  is given by

$$C_D = \frac{2 \sin \gamma (F_B - F_g)}{\rho S v_g^2}, \quad (19)$$

$C_D$  was bin averaged in 0.5° intervals if the number of data points was 2000 or greater in each bin (Fig. 4g). This threshold of 2000 is discussed in section 4b. The quadratic curve was a reasonable fit to the observed relationship (the red curve in Fig. 4h), with  $C_{D0}$  and  $C_{D1}$  determined as 0.18 and 5.92 rad $^{-2}$ , respectively, during this mission.

The total lift coefficient  $a$  was then estimated so that the flight model gives the observed pitch–AOA relationship derived from the ADCP (Fig. 4f). AOA from the ADCP was averaged into 0.5° bins of pitch angle, and the bins whose number of data points was less than 2000 were also excluded (Fig. 4e). The resultant  $a$  was found to be 5.4 rad $^{-1}$  for our Slocum glider (the red curve in Fig. 4f). Note that  $c$  and  $V_{\text{GL}}$  did not change significantly ( $4.6 \times 10^{-10}$  Pa $^{-1}$  and 68.2 L, respectively) if they were reevaluated by the MEA10 method with the  $C_{D1}$  and  $a$  we obtained. The flight model with our estimated lift and drag coefficients better captured the observed pitch–AOA relationship than that with the MEA10's coefficients (the black solid curve in Fig. 4f based on  $C_{D0} = 0.19$  determined by the MEA10 method with MEA10's  $C_{D1}$  and  $a$ ). MEA19 recently updated  $C_{D1}$  and  $a$  to be 10.5 rad $^{-2}$  and 7.5 rad $^{-1}$ , respectively, using their Slocum gliders and attaching either an EM current sensor or an ADCP. However, their updated coefficients would not give a closer agreement between the modeled AOA and the AOA estimated by our ADCP data (black dashed line in Fig. 4f based on  $C_{D0} = 0.16$  determined by the MEA10 method with MEA19's  $C_{D1}$  and  $a$ ). The modeled AOA with the MEA10's and MEA19's coefficients

were smaller than that with our coefficients by 0.5° and 1.3°, respectively, on average for the nominal pitch angle of 20°–30° (Fig. 4f).

The lift and drag coefficients of this study also gave a reasonable estimate for the vertical and along-glider velocity time series (Figs. 5a–c). The glider's speed through water,  $v_g$ , derived from the flight model [Eq. (8)] agreed well with that from the ADCP ( $v_g = v_p/\cos \alpha$ ): using all data points after being processed and screened as in section 2b(2), the mean value of  $v_{g,\text{FLM}}/v_{g,\text{ADCP}}$  was 1.01, and 95% of the data were between 0.92 and 1.11 (Fig. 5d). Since the estimation of turbulent energy dissipation rate depends on  $v_g^{-4}$  (e.g., Lueck et al. 1997),  $v_g^4$  derived from the flight model was also compared with that from the ADCP at each data point. Using the obtained coefficients, the histogram of  $(v_{g,\text{FLM}}/v_{g,\text{ADCP}})^4$  was well fit by a lognormal distribution (Fig. 5e). The mean value became 1.06, and 95% of the data were between 0.71 and 1.50, indicating an unbiased estimation of energy dissipation rate between ADCP and the flight model. The along-glider velocity estimated by the MEA10's and MEA19's coefficients was larger by 2% and 4% on average, respectively, than that estimated by the coefficients of this study (Fig. 5c). The use of MEA10's (MEA19's) coefficients instead of this study's would result in the fractional difference of 7% (17%) on average in estimating energy dissipation rate.

#### b. Estimation of lift and drag coefficients of the SeaExplorer

To our knowledge, the lift and drag coefficients of the SeaExplorer have yet to be documented. This subsection estimates the coefficients using the same method presented in section 3a. Since  $C_{D1}$  and  $a$  required for the MEA10 method were unknown for the SeaExplorer, the following iterative steps were made:

- First, let the initial values of  $C_{D1}$  and  $a$  be those used by MEA10 (i.e.,  $C_{D1} = 2.88$  rad $^{-2}$  and  $a = 6.1$  rad $^{-1}$ ).
- Then estimate  $C_{D0}$ ,  $c$ , and  $V_{\text{GL}}$  by the MEA10 method.

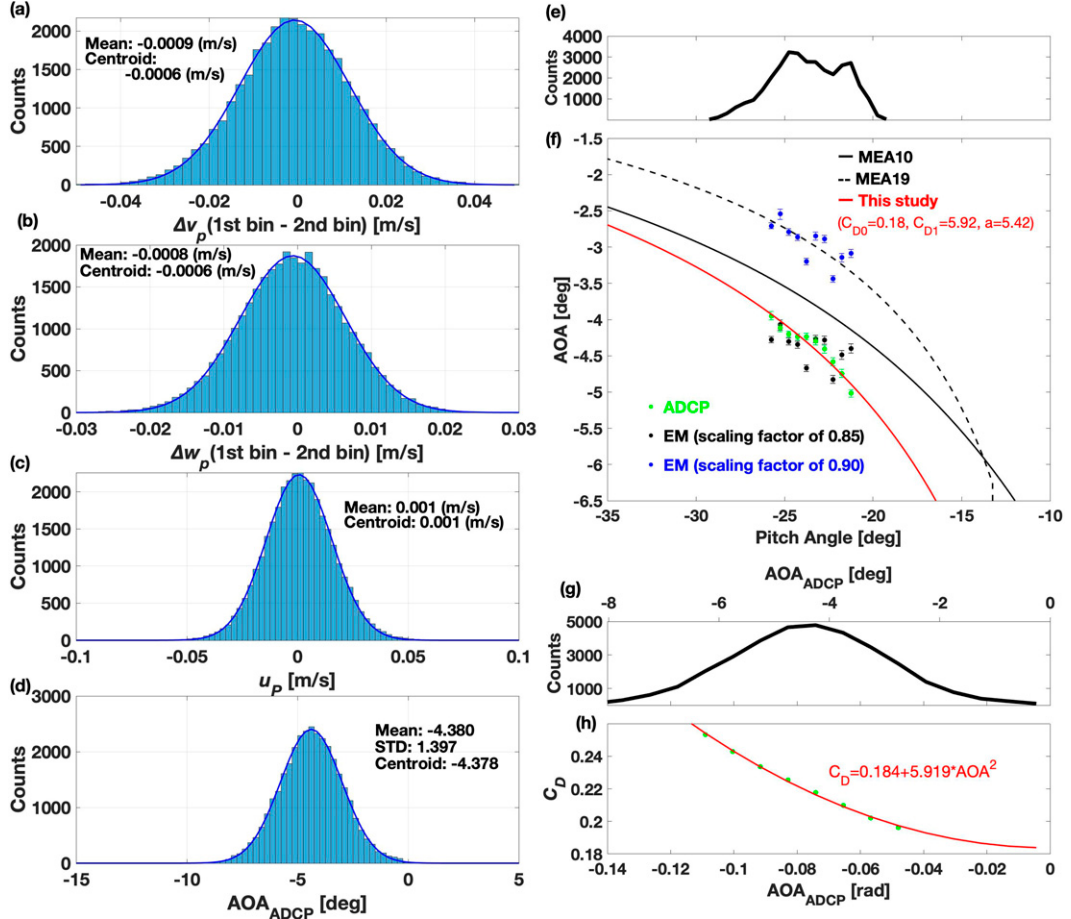


FIG. 4. Histograms of (a) the difference in  $v_p$  between the first and second closest bin, (b) the difference in  $w_p$  between the first and second closest bins, (c) cross-glider velocity  $u_p$ , and (d) AOA derived from the ADCP for the Slocum mission. A blue curve is the Gaussian function fitted to each histogram whose centroid value is shown in each panel. (e) The number of data points used for analysis at each 0.5° pitch bin for the Slocum mission. (f) Green dots are the observed pitch–AOA relationship averaged in each 0.5° bin from the Slocum ADCP. Black and blue dots are the same but using the EM sensor data corrected by a scale factor of 0.85 and 0.90, respectively. An error bar denotes 95% confidence interval at each bin estimated by the bootstrap method (Efron and Gong, 1983). Red, solid black, and dashed black curves are the modeled  $AOA_{FLM}$  using the drag and lift coefficients of this study, MEA10, and MEA19, respectively. (g) The number of data points used for analysis at each 0.5° AOA bin derived from the ADCP. (h) The green dots are the observed AOA– $C_D$  relationship averaged in each 0.5° bin for the Slocum mission. The red curve is a fitted quadratic function denoted by the formula in the panel.

- (iii) Using the derived  $c$  and  $V_{GL}$ , the optimum lift and drag coefficients are derived by the method described in section 3a.
- (iv) The obtained  $C_{D1}$  and  $a$  are then used to derive  $C_{D0}$ ,  $c$ , and  $V_{GL}$  by the MEA10 method.
- (v) Iterate steps (iii) and (iv) until the fractional changes in  $C_{D0}$ ,  $c$ , and  $V_{GL}$  between iterations are all less than 5%. The resulting lift and drag coefficients are then used in this section.

In the above procedure, surface area of the wings,  $S$ , was set to be 0.14 m<sup>2</sup> for the SeaExplorer, whose wing has 2 plates on each side (Fig. 1c). Using both descent and ascent data, the final values of  $c$  and  $V_{GL}$  are  $5.3 \times 10^{-10}$  Pa<sup>-1</sup> and 62.0 L, respectively.

The mean  $|w_g|$  derived from the ADCP was 0.14 m s<sup>-1</sup> for the descent and 0.21 m s<sup>-1</sup> for the ascent (Table 2). The mean velocity difference between the first and second nearest bins was  $-7 \times 10^{-4}$  and  $-6 \times 10^{-4}$  m s<sup>-1</sup> for  $v_p$  and  $w_p$ , respectively, for the descent and  $-4 \times 10^{-3}$  and  $-1 \times 10^{-3}$  m s<sup>-1</sup> for the ascent (Figs. 6a,b). The histograms were well fit by a Gaussian distribution, and the mean current shear was much smaller than the mean  $v_p$  and  $w_p$  (Table 2), indicating that it is reasonable to assume that the current shear was not large enough to affect the glider speed through water if we consider the average values. The mean cross-glider velocity  $u_p$  was also about 1% of the mean  $v_p$  (Table 2), and the histograms were well fit by Gaussian distributions (Fig. 6c). Therefore, the ADCP is considered to reasonably capture the glider motion

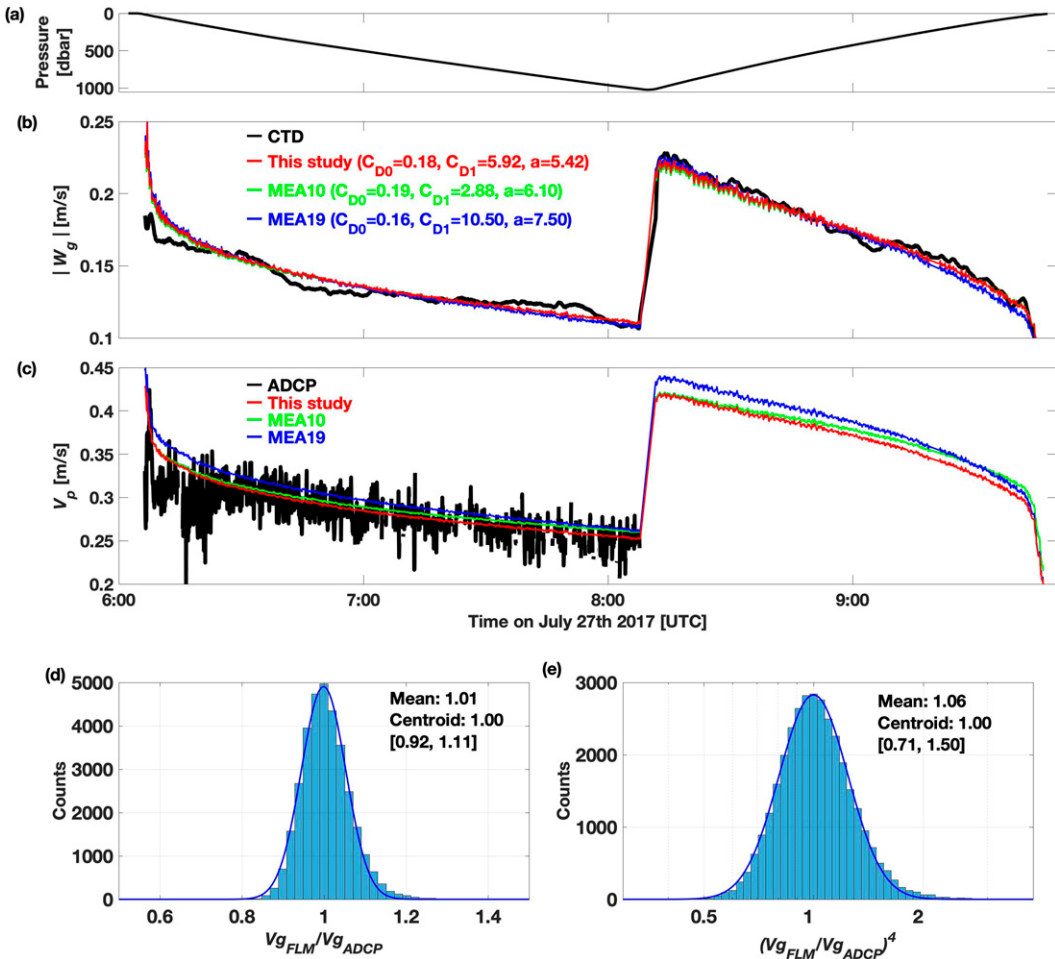


FIG. 5. Time series of (a) pressure, (b) vertical velocity  $w_g$ , and (c) along-glider velocity  $v_p$  for the Slocum mission on 27 Jul 2017. The red, green, and blue lines in (b) and (c) are derived from the flight model using the drag and lift coefficients of this study, MEA10, and MEA19, respectively. The green line in (b) is under the red and/or blue lines.  $C_{D0}$  of MEA10 and MEA19 shown in (b) are calculated by the MEA10 method using our dataset with  $C_{D1}$  and  $a$  reported by MEA10 and MEA19, respectively. (d) A histogram of the ratio of  $v_g$  derived from the ADCP to that from the flight model,  $v_{g\_FLM}/v_{g\_ADCP}$ , using the drag and lift coefficients of this study shown in (b) for the Slocum mission. (e) As in (d), but for  $(v_{g\_FLM}/v_{g\_ADCP})^4$ . The horizontal scale of (e) is logarithmic.

through water for the SeaExplorer as well. The average of AOA was  $-7.7^\circ$  and  $5.1^\circ$  during the descent and ascent, respectively (Fig. 6d). The histogram deviated from a Gaussian distribution since the glider's speed and attitude (i.e., pitch angle) changed with depth during the flight (Fig. 3a).

Using the above-mentioned procedure, the observed relationship between the AOA estimated by the ADCP and total drag coefficient  $C_D$ , averaged in  $0.5^\circ$  bins, was fit by the quadratic function [Eq. (7)] if the number of data points was 200 or greater in each bin (Fig. 6e). This threshold of 200 is discussed in section 4a. The resultant  $C_{D0}$  and  $C_{D1}$  were determined as 0.19 and  $5.0 \text{ rad}^{-2}$ , respectively (red curve in Fig. 6f). Using the estimated  $C_{D0}$  and  $C_{D1}$ , the total lift coefficient,  $a$ , was estimated as  $4.0 \text{ rad}^{-1}$  to best describe the observed pitch–AOA relationship (red and blue curves in Fig. 6h) which had 200 or greater data points at each  $0.5^\circ$  bin of pitch angle (Fig. 6g).

The flight model with our lift and drag coefficients also gave a reasonable estimate for the vertical and along-glider velocity time series (Figs. 7a–c). From these coefficients, the mean value of  $v_{g\_FLM}/v_{g\_ADCP}$  was 1.01, and 95% of the data were between 0.91 and 1.11 based on all data points after being processed and screened as in section 2b(2) (Fig. 7d). The histogram of  $(v_{g\_FLM}/v_{g\_ADCP})^4$  also had a fair agreement with a lognormal distribution centered at 1.05 (Fig. 5i), and 95% of the data was between 0.69 and 1.50, indicating an unbiased estimation of energy dissipation rate between ADCP and the flight model. We would like to note that the result does not change significantly even if the above procedure is done separately for the descent and ascent;  $C_{D0}$  and  $C_{D1}$  were determined as 0.21 and  $4.5 \text{ rad}^{-2}$ , respectively, for descent (Fig. 8a) and 0.19 and  $5.1 \text{ rad}^{-2}$  for ascent (Fig. 8b) based on the same  $c$  and  $V_{GL}$  used in this section. Also, the total lift coefficient

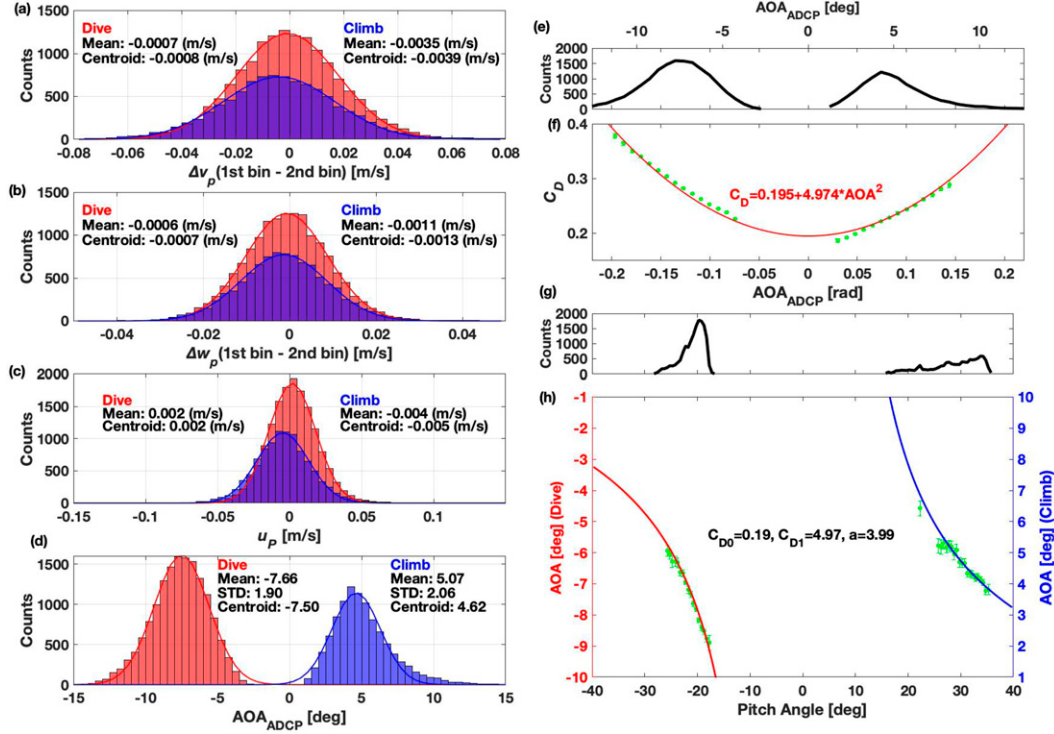


FIG. 6. Histograms of (a) the difference in  $v_p$  between the first and second closest bins, (b) the difference in  $w_p$  between the first and second closest bin, (c) cross-glider velocity  $u_p$ , and (d) AOA derived from the ADCP for the SeaExplorer mission. Histograms for descent (ascent) data are denoted by red (blue) color, and a red (blue) curve is the Gaussian function fitted to each histogram whose centroid value is shown in each panel for descent (ascent). (e) The number of data points used for analysis at each  $0.5^\circ$  AOA bin derived from the ADCP. (f) The green dots are the observed AOA– $C_D$  relationship averaged in each  $0.5^\circ$  bin for the SeaExplorer mission. The red curve is a fitted quadratic function denoted by the formula in the panel. (g) The number of data points used for analysis at each  $0.5^\circ$  pitch bin for the SeaExplorer mission. (h) Green dots are the observed pitch–AOA relationship averaged in each  $0.5^\circ$  bin from the SeaExplorer ADCP. An error bar denotes 95% confidence interval at each bin estimated by the bootstrap method (Efron and Gong, 1983). The modeled AOA using the drag and lift coefficients of this study is shown as solid curves, and the left (right) axis is used for the descent (ascent) data denoted by red (blue) color.

was estimated to be  $4.0 \text{ rad}^{-1}$  for both descent and ascent (the red curves in Figs. 8c,d). For the typical pitch range of  $20^\circ$ – $30^\circ$ , the resultant AOA would differ only by about  $0.1^\circ$  from that derived from both descent and ascent data.

#### 4. Discussion

##### a. Uncertainties in estimating lift and drag coefficients

This study proposes a method to estimate optimum lift and drag coefficients for underwater gliders based on the AOA derived from the ADCPs. The technical hurdle of our method is to obtain accurate vertical-glider velocity  $w_p$ , which is about  $2 \text{ cm s}^{-1}$  (Figs. 2f, 3c). To get the AOA precision to  $5\%$ ,  $w_p$  precision should be  $0.1 \text{ cm s}^{-1}$ . Since a single ping of the RDI ADCP has a precision of about  $5 \text{ cm s}^{-1}$  (MEA19), the rough estimate of the number of pings that is necessary to be averaged would be  $(5/0.1)^2 = 2500$  so that the above-mentioned precision is achieved for the Slocum glider. Considering that our velocity data were 10-ping ensembles recording every 3–4 s, roughly 250 ensembles (i.e.,  $\sim 20$  min) are necessary to be

averaged. As for our Nortek ADCP, a 4-ping ensemble was taken every second, and the velocity data were recorded as the average of 10 ensembles. Since the precision of a single ensemble beam velocity<sup>2</sup> was  $1.04 \text{ cm s}^{-1}$ , the precision of along-glider and vertical-glider velocity was  $2$  and  $1 \text{ cm s}^{-1}$ , respectively, by accounting for error propagation. Taking the former value, about 400 ensembles ( $\sim 5$  min) are then necessary to be averaged to get a precision of  $0.1 \text{ cm s}^{-1}$  for the SeaExplorer. Therefore, since the time series of AOA derived from the ADCP is expected to be noisy, a large number of data points should be averaged to obtain a precise AOA time series, which would significantly reduce the temporal resolution of AOA time series. Due to this limitation, MEA19 used the time series of horizontal gliding speed from the ADCP and obtained the total lift coefficient by matching the measured and modeled horizontal glider motion. TEA17, who calculated AOA by

<sup>2</sup> This precision was derived from the GETPRECISION command of the ADCP.

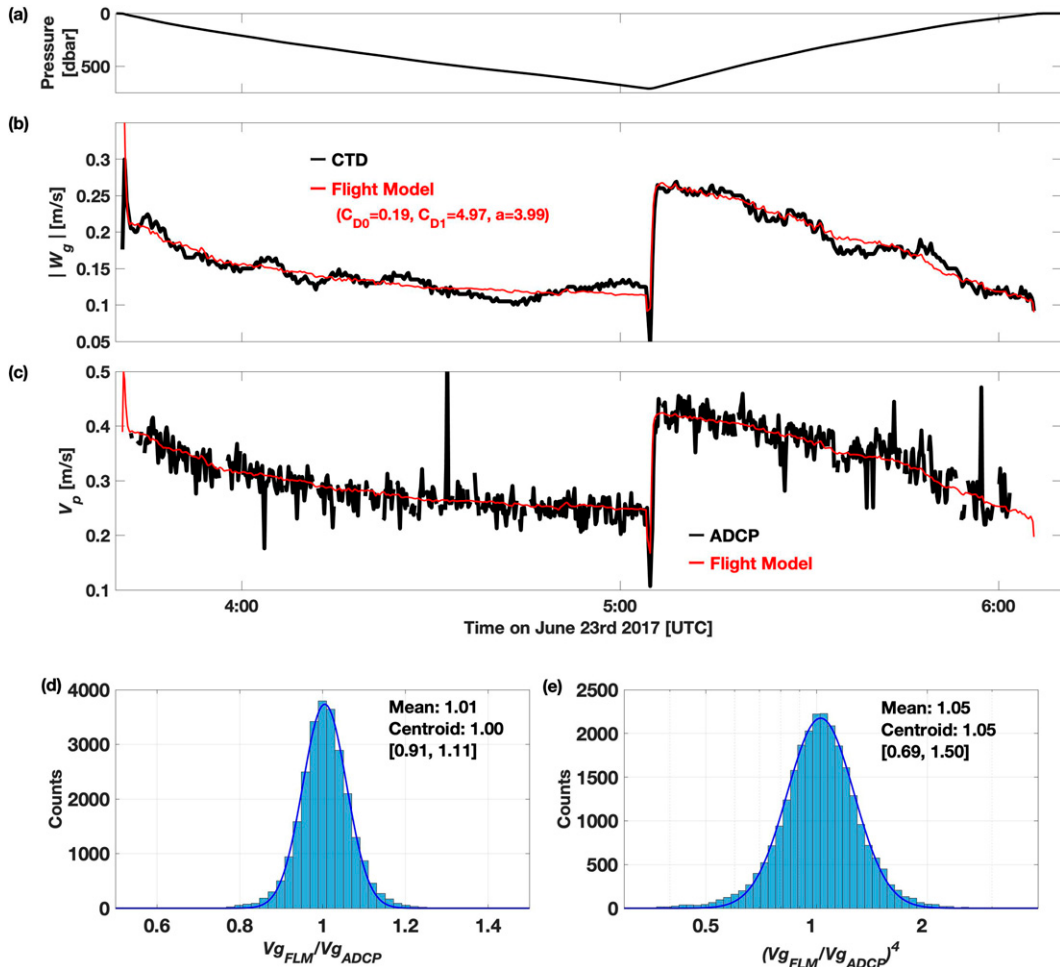


FIG. 7. Time series of (a) pressure, (b) vertical velocity  $w_g$ , and (c) along-glider velocity  $v_p$ , for the SeaExplorer mission on the 23 Jun 2017. The red line in (b) and (c) is derived from the flight model using the drag and lift coefficients of this study. (d) A histogram of the ratio of  $v_g$  derived from the ADCP to that from the flight model,  $v_{g\_FLM}/v_{g\_ADCP}$ , using the drag and lift coefficients of this study shown in (b) for the SeaExplorer mission. (e) As in (d), but for  $(v_{g\_FLM}/v_{g\_ADCP})^4$ . The horizontal scale of (e) is logarithmic.

$\alpha = \arctan(w/u_{\text{fwd}}) - \theta$ , also noted that their AOA time series were quite noisy, so their time series were averaged over each dive to obtain AOA time series with respect to the dive number.

Our method did not rely on the time series of AOA; alternatively, we examined statistical properties derived from the whole mission of each glider and conducted regression analysis to estimate the lift and drag coefficients that best explain the statistical relationship between, for instance, AOA and pitch angle (e.g., Figs. 4f, 6h). Although our method does not take the time series viewpoint, since AOA derived from the ADCPs contains the above-mentioned instrumental noise, a large number of velocity data with the same flight conditions such as oil volume and battery position are also required to obtain the reliable statistical relationship that represents the mission. To remove bins that have larger uncertainty in estimating the mean values of AOA and the total drag coefficient  $C_D$ , the histogram of each  $0.5^\circ$  pitch/AOA bin was examined (Fig. 9). If the bin contains a sufficient number of data points,

then the histogram tends to be well fit by a single Gaussian distribution, and the mean value is close to the centroid of the fitted Gaussian distribution, as shown in Fig. 9a for AOA of the Slocum in a  $0.5^\circ$  pitch bin. The difference in AOA between the mean value and the centroid was typically less than  $0.1^\circ$  for bins containing more than 2000 data points (Fig. 9b). For the SeaExplorer, the histogram was slightly skewed from the Gaussian distribution toward larger AOA, which resulted in larger AOA difference between the mean and the centroid (Fig. 9c). The mean-centroid difference was especially large when the bins contained less than 200 data points (Fig. 9d), and these bins were removed from estimating the total lift coefficient in section 3b (Figs. 6h, 8c,d). The histogram of  $C_D$  was slightly skewed from the Gaussian toward larger  $C_D$  for the Slocum glider (Fig. 9e), and the mean-centroid difference was less than 0.005 for AOA bins containing 2000 data points or greater (Fig. 9f). The histogram was also slightly skewed for the SeaExplorer (Fig. 9g), and the mean-centroid

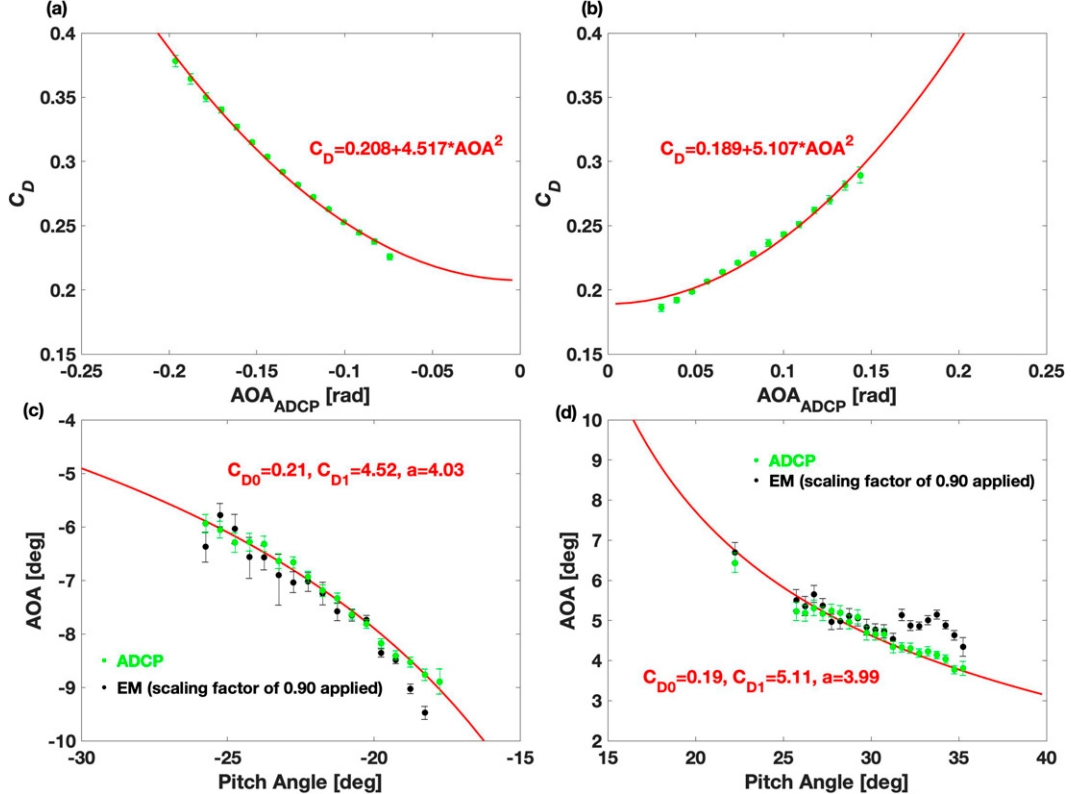


FIG. 8. (a) The green dots are the observed AOA– $C_D$  relationship averaged in each  $0.5^\circ$  bin using only the descent casts of SeaExplorer mission. The red curve is a fitted quadratic function denoted by the formula in the panel. (b) As in (a), but for the ascent casts. (c) Green dots are the observed pitch–AOA relationship averaged in each  $0.5^\circ$  bin from the descent data of SeaExplorer ADCP. An error bar denotes 95% confidence interval at each bin estimated by the bootstrap method (Efron and Gong, 1983). The modeled AOA using the drag and lift coefficients from the descent casts only is shown as a red curve. Black dots are the pitch–AOA relationship using the EM sensor data corrected by a scale factor of 0.90. (d) As in (c), but for the ascent casts.

difference in  $C_D$  exceeded 0.01 when the number of data points was less than 200 (Fig. 9h). In this study, bins that have less than 2000 (200) data points were removed from the regression analysis for the Slocum (SeaExplorer) mission in section 3. We also note that some of the noise in our velocity data appeared as spikes (Figs. 2, 3), which sometimes remained after the data selection procedures in section 2. However, the results in section 3 were not significantly changed even if the large spikes were removed from our velocity data by applying a median filter (see appendix D).

Another uncertainty in our estimation of lift and drag coefficients is the influence of roll. If the roll is not zero, then the lift force is not precisely pointing up. The roll of  $5^\circ$  would result in about 0.4% difference between the total and the vertical component of the lift force. The sideslip angle, which is the difference between the heading and the glider's path in the horizontal plane (TEA17), also affects the estimation. The mean sideslip angle derived from  $\arctan(u_p/v_{fwd})$  (TEA17) was less than  $1.0^\circ$  for both our Slocum and SeaExplorer missions. Although the influences of roll and sideslip angle are considered insignificant for our missions, since there are above-mentioned uncertainties in obtaining the statistical properties and estimating the lift and drag

coefficients, it is important to examine whether our results from the regression analysis are also consistent with those obtained from different methods. In the following sections, a method proposed by MEA19 was applied to our Slocum and SeaExplorer dataset to get the total lift and the parasite drag coefficient and compared the resultant AOA with those obtained in section 3.

#### b. Estimation of lift and drag coefficients from MEA19 method

Since both the lift and drag coefficients cannot be determined at the same time solely from matching the measured and modeled vertical motion, MEA19 also used the glider's speed through water derived from the ADCP as an additional constraint and obtained the total lift coefficient  $a$  by matching the modeled and measured horizontal motion of the glider. Since the ADCP bottom-track data, which MEA19 used for getting the glider's speed through water, were unavailable for this study, we instead used the along-glider velocities at the nearest bin under the assumption of no current shear (Figs. 4a, 6a). Using this information,  $C_{D0}$  and  $a$  were estimated following MEA19 (hereafter, this procedure is called the modified MEA19 method):

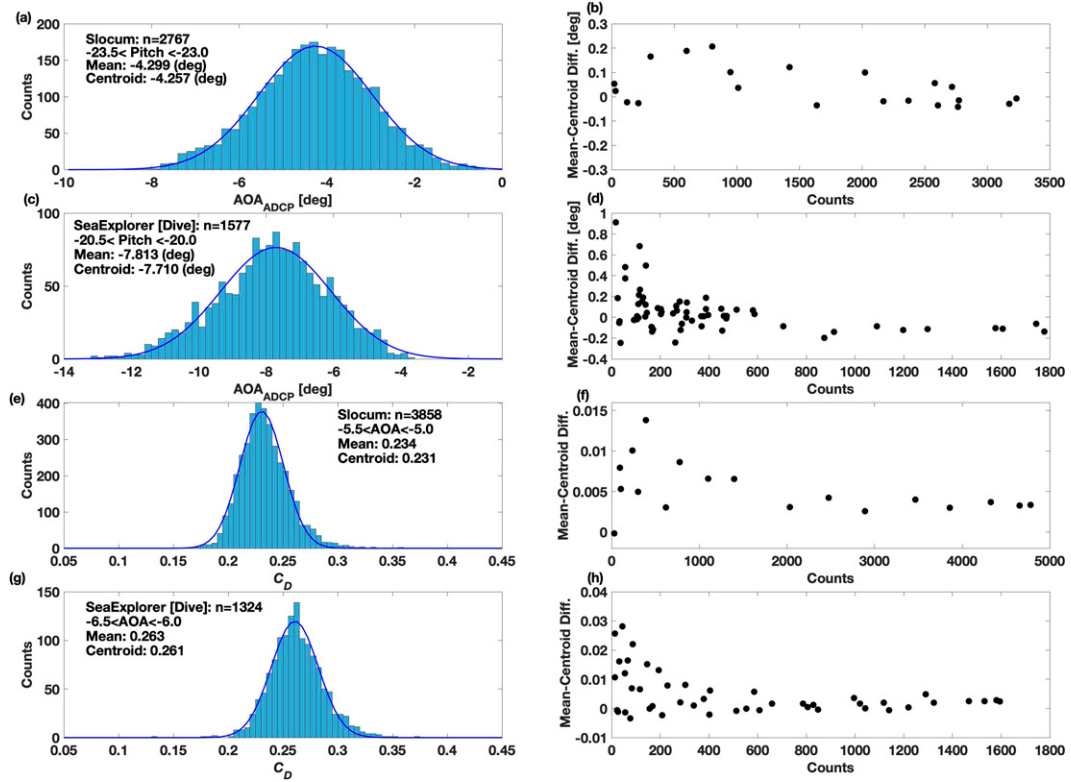


FIG. 9. (a) A histogram of AOA derived from the Slocum ADCP for the pitch angle of 22.5°–23.0°. (b) A scatterplot of mean-centroid difference in AOA and the number of data points averaged at each 0.5° pitch bin for the Slocum mission. (c),(d) As in (a) and (b), respectively, but for the SeaExplorer mission. (e) A histogram of calculated  $C_D$  derived from the Slocum ADCP for the AOA range of 4.5°–5.0°. (f) A scatterplot of mean-centroid difference in  $C_D$  and the number of data points averaged at each 0.5° AOA bin for the Slocum mission. (g),(h) As in (e) and (f), respectively, but for the SeaExplorer mission. Both descent and ascent data are included for the SeaExplorer mission. The blue curve in (a), (c), (e), and (g) is the Gaussian function fitted to each histogram whose centroid value is shown in each panel.

- M1) First, estimate  $C_{D0}$ ,  $c$ , and  $V_{GL}$  by the [MEA10](#) method for preset values of lift coefficient  $a$ .
- M2) The optimum set of  $a$  and  $C_{D0}$  is chosen that minimizes the difference between the modeled and ADCP-measured glider speed through water:

$$CF2 = \sum (v_g - v_p / \cos \alpha)^2, \quad (20)$$

where  $v_g$  and  $\alpha$  is derived from the flight model, and the summation is over all the analyzed ADCP data points of each glider's mission. In this calculation,  $C_{D1}$  was set to be 5.9 and 5.0  $\text{rad}^{-2}$  for the Slocum and SeaExplorer, respectively, which were derived in [section 3](#).

[Figure 10a](#) is the result of the above procedure for the preset values of lift coefficient for the Slocum glider. CF2 was minimized when  $a = 5.5 \text{ rad}^{-1}$ , and the corresponding  $C_{D0}$  was 0.186, which agreed with those obtained by this study ( $C_{D0} = 0.184$  and  $a = 5.4 \text{ rad}^{-1}$ ) within a factor of 5%. The mean difference in the modeled AOA between the modified [MEA19](#) method and this study was also less than 0.1° for typical pitch angle of 20°–30°. Similar agreement was also obtained for

the SeaExplorer: CF2 was minimized when  $a = 3.9 \text{ rad}^{-1}$ , and the corresponding  $C_{D0}$  was 0.192 ([Fig. 10b](#)). The resultant mean difference in the modeled AOA was also about 0.1° for pitch angle of 20°–30°. These results indicate that the lift and drag coefficients obtained by the regression method of this study also satisfied the vertical and horizontal constraints of the glider motion.

## 5. Concluding remarks

This study demonstrates a method to estimate the lift and drag coefficients of the underwater glider flight model based on the knowledge of AOA obtained by an ADCP. AOA is estimated using the along-glider and vertical-glider velocities from the nearest bin to the transducer. Since the mean current shear is sufficiently small, the ADCP velocities reasonably capture the glider's speed through water, on average. The lift and drag coefficients of the flight model are derived so that the flight model can best explain the observed pitch-AOA relationship. Thus, the resultant coefficients give an unbiased estimation of the energy dissipation rate between the ADCP and the flight model. If enough data are collected,

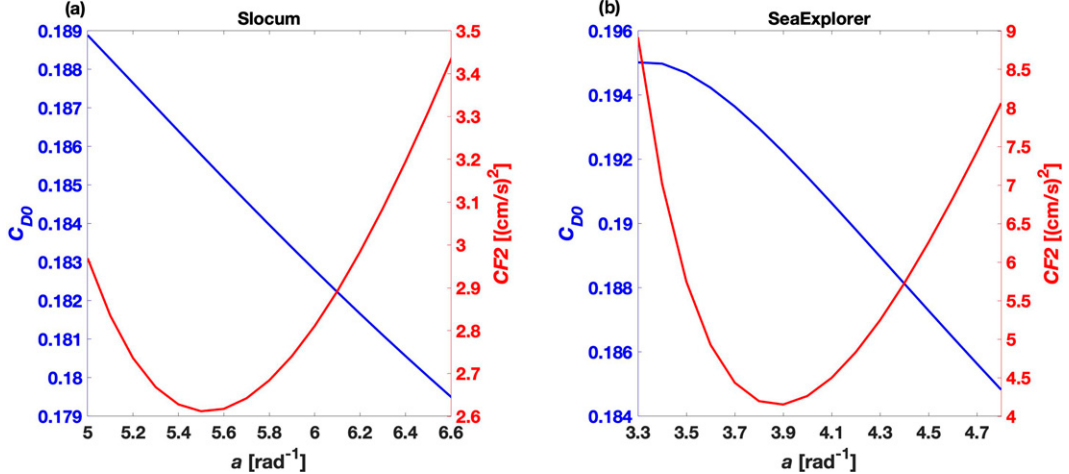


FIG. 10. (a) The variation of  $C_{D0}$  and CF2 with respect to the total lift coefficient  $a$  obtained by the modified MEA19 method for the Slocum mission. (b) As in (a), but for the SeaExplorer mission.

the influence of instrumental noise of the ADCP measurement can be reduced, and the resultant lift and drag coefficients can satisfy the vertical and horizontal constraints of the glider motion.

This method was applied to the SeaExplorer glider to estimate the lift and drag coefficients for the first time. The resultant lift and drag coefficients also satisfied the vertical and horizontal constraints, and the modeled AOA well captured the observed pitch-AOA relationship derived from the ADCP. The modeled AOA did not differ by more than 5% from that with the coefficients obtained by constraining the vertical and horizontal glider motion. These results suggest that our regression method to estimate the lift and drag coefficient for underwater gliders can be applied to many types of underwater gliders with an ADCP and give a statistical insight into the flight characteristics of underwater gliders.

Since the steady-state flight model can estimate the AOA solely from the pitch angle monitored by the glider [Eq. (1)], the information of lift and drag coefficients would be valuable for dead-reckoning calculations and improve glider navigation. Also, the knowledge of AOA as well as these coefficients provides the better estimation of glider's speed through water, which would facilitate the quantification of mixing intensity by ocean microstructure gliders that do not have velocity sensors installed. Since velocity measurements from the ADCP can also yield absolute velocity and current shear profiles (e.g., TEA17; de Fommervault et al. 2019), ocean microstructure gliders with ADCP would also provide a useful tool to collect concurrent fine and microstructure data and promote our understanding of the mixing processes in the ocean.

**Acknowledgments.** We thank the officers, crews, and on-board scientists of the R/V *Wakataka-maru* WK1707A and WK1708F cruises and the R/V *Shinsei-maru* KS1705 cruise for help deploying and recovering the glider. We thank

Dr. Orens de Fommervault for providing information about the ADCP data processing for SeaExplorer. We also thank Dr. Rolf Lueck from Rockland Scientific for his invaluable comments on this manuscript. We appreciate Dr. Lucas Merckelbach for his thoughtful review and invaluable suggestions on this study. We also thank the editor and two anonymous reviewers for their invaluable comments. This study was supported by Grants-in-Aid for Scientific Research [MEXT KAKENHI JP15H05818, JP21H04921, JP22H05201, and JP22H05205] and the Cooperative Program (No. 147, 2020, and No. 151, 2021) of the Atmosphere and Ocean Research Institute, The University of Tokyo.

**Data availability statement.** The observational data used for the analysis of this study are openly available at [https://oeg.aori.u-tokyo.ac.jp/omix/TanakaT\\_etal\\_FLM\\_2021](https://oeg.aori.u-tokyo.ac.jp/omix/TanakaT_etal_FLM_2021).

## APPENDIX A

### Cubic Solution for Eq. (1)

This study solved Eq. (1) as follows. The Taylor series expansion of  $\sin(\theta + \alpha)$  and  $\cos(\theta + \alpha)$  about  $\theta$  gives

$$\begin{aligned} \sin(\theta + \alpha) &= \sin(\theta) + \cos(\theta) \times \alpha - \sin(\theta)/2 \times \alpha^2 \\ &\quad - \cos(\theta)/6 \times \alpha^3 + \dots, \end{aligned} \quad (\text{A1})$$

and

$$\begin{aligned} \cos(\theta + \alpha) &= \cos(\theta) - \sin(\theta) \times \alpha - \cos(\theta)/2 \times \alpha^2 \\ &\quad + \sin(\theta)/6 \times \alpha^3 + \dots. \end{aligned} \quad (\text{A2})$$

Rewriting Eq. (1) as

$$a \sin(\theta + \alpha) \times \alpha = \cos(\theta + \alpha) \times (C_{D0} + C_{D1}\alpha^2), \quad (\text{A3})$$

and then substituting (A1) and (A2) into (A3) yields

$$\begin{aligned}
& a[\sin(\theta) + \cos(\theta) \times \alpha - \sin(\theta)/2 \times \alpha^2 - \cos(\theta)/6 \\
& \times \alpha^3 + \dots] \times \alpha = [\cos(\theta) - \sin(\theta) \times \alpha - \cos(\theta)/2 \\
& \times \alpha^2 + \sin(\theta)/6 \times \alpha^3 + \dots] \times (C_{D0} + C_{D1}\alpha^2), \quad (\text{A4})
\end{aligned}$$

where  $a = a_h + a_w$ . Finally, collecting the powers of  $\alpha$  through third order gives

$$\begin{aligned}
0 &= \sin(\theta) \times (C_{D0}/6 - C_{D1} + a/2) \times \alpha^3 - \cos(\theta) \\
&\times (C_{D0}/2 - C_{D1} + a) \times \alpha^2 - \sin(\theta) \\
&\times (C_{D0} + a) \times \alpha + C_{D0} \times \cos(\theta). \quad (\text{A5})
\end{aligned}$$

This study solved Eq. (A5) to obtain  $\alpha$ . The cubic solutions have a fractional error of about 0.8% at  $5^\circ$  in  $\alpha$ .

## APPENDIX B

### The Offset of Tilt Sensors

The offset of tilt sensors (i.e., pitch and roll angles) was determined so that the vertical velocity  $w_g$  derived from the ADCP and the pressure sensor matched (TEA17). Since the velocity data were recorded in Earth coordinates for the Slocum glider, the data were first transformed to the glider-coordinate system using the heading  $\varphi$ , pitch  $\theta$ , and roll  $\zeta$  recorded by the ADCP:

$$u_1 = (v \cos \varphi + u \sin \varphi) \cos \theta + w \sin \theta, \quad (\text{B1})$$

$$\begin{aligned}
u_2 &= (-v \sin \varphi + u \cos \varphi) \cos \zeta - [(-v \cos \varphi \\
&- u \sin \varphi) \sin \theta + w \cos \theta] \sin \zeta, \quad (\text{B2})
\end{aligned}$$

$$\begin{aligned}
u_3 &= (-v \sin \varphi + u \cos \varphi) \sin \zeta + [(-v \cos \varphi \\
&- u \sin \varphi) \sin \theta + w \cos \theta] \cos \zeta, \quad (\text{B3})
\end{aligned}$$

where  $u$ ,  $v$ , and  $w$  are eastward, northward, and vertical velocities, respectively, recorded in the nearest bin of ADCP. Then  $u_1$ ,  $u_2$ , and  $u_3$  were rotated back to the Earth coordinates using the corrected pitch and roll angles to obtain  $w_g$ :

$$\begin{aligned}
w_{g\_ADCP} &= -\{u_1 \sin(\theta + \theta') + [-u_2 \sin(\zeta + \zeta')] \\
&+ u_3 \cos(\zeta + \zeta')] \cos(\theta + \theta')\}, \quad (\text{B4})
\end{aligned}$$

where  $\theta'$  and  $\zeta'$  are the offset of pitch and roll angle, respectively. In this equation,  $w_{g\_ADCP}$  is negative during descent, so the sign of  $w_g$  derived from the navigation depth sensor is reversed throughout this appendix. As described in section 2b, the ADCP data were excluded from analysis if any of R1, R2, R3, or R4 were not met. The data with positive  $w_p$  were also excluded (section 2b). The time delay of the ADCP data (9 s) was adjusted, and the sound speed correction was also applied. Then, after extracting the descent data by  $\theta + \theta' < 0^\circ$  and  $w_g < -0.05 \text{ m s}^{-1}$ , the offset was determined so that the mean square difference between  $w_{g\_ADCP}$  and  $w_g$  derived from the depth sensor was minimized.

For the SeaExplorer glider, which recorded the velocity data in beam coordinates, the data were first transformed to the glider coordinates by

$$\begin{pmatrix} u_1 \\ u_2 \\ u_3 \end{pmatrix} = \begin{pmatrix} 1.3563 \operatorname{sgn}(\theta) & -0.5055 \operatorname{sgn}(\theta) & -0.5055 \operatorname{sgn}(\theta) \\ 0 & -1.1831 & 1.1831 \\ 0 & 0.5517 & 0.5517 \end{pmatrix} \begin{pmatrix} v_1 \text{ or } v_3 \\ v_2 \\ v_4 \end{pmatrix}, \quad (\text{B5})$$

where  $v_1$ ,  $v_2$ ,  $v_3$ , and  $v_4$  are velocities measured by each beam, and  $v_1$  ( $v_3$ ) is used for descent (ascent). Then they were transformed to the Earth coordinates to obtain  $w_{g\_ADCP}$  by Eq. (B4). As described in section 2c, the ADCP data were analyzed if all of R1, R2, R4, and R5 were met. The time difference between the navigation and the ADCP clock (12 s) was adjusted, and the sound speed correction was applied before determining the pitch and roll offset by the same method used for the Slocum.

Before correcting the offset,  $w_g - w_{g\_ADCP}$  was negatively biased for the Slocum glider and positively biased for the SeaExplorer (Figs. B1a,c) by 2.6 and 2.9  $\text{mm s}^{-1}$ , respectively, on average. The computed offset of pitch and roll angle was  $-0.5^\circ$  and  $5.6^\circ$ , respectively, for the Slocum glider and  $0.6^\circ$  and  $3.0^\circ$  for the SeaExplorer glider (Figs. B1b,d). After correcting the offset, the mean difference between  $w_{g\_ADCP}$  and  $w_g$  derived from the navigation depth sensor was less than  $1 \text{ mm s}^{-1}$ . It is noted that to correct the influence of the roll offset on the cross- and vertical-glider velocities of the Slocum glider,  $u_p$  [Eq. (12)] and  $w_p$  [Eq. (14)] were further rotated using the recorded roll angle,  $\zeta$ , and then were rotated back using the corrected roll angle,  $\zeta + \zeta'$ . The final forms of  $u_p$  and  $w_p$  were

$$u_p = -u_2 \cos(\zeta + \zeta') - u_3 \sin(\zeta + \zeta'), \quad (\text{B6})$$

and

$$w_p = u_2 \sin(\zeta + \zeta') - u_3 \cos(\zeta + \zeta'), \quad (\text{B7})$$

respectively, and they were used for calculating AOA by Eq. (15).

## APPENDIX C

### Estimation of Lift and Drag Coefficients based on the Velocity Data from Deeper Bins

This study used the ADCP velocity data from the nearest bin to calculate AOA and estimate the lift and drag coefficients as the influence of current shear is considered to be minimized (section 3). MEA19, who used the same RDI ADCP as ours for the Slocum glider, noted that the velocity from the nearest bin is different from those from deeper bins, and they excluded the nearest bin from their analysis. In this appendix, the velocity data from deeper bins are also analyzed for both the Slocum and SeaExplorer mission, and the results are compared with those obtained from the nearest bin.

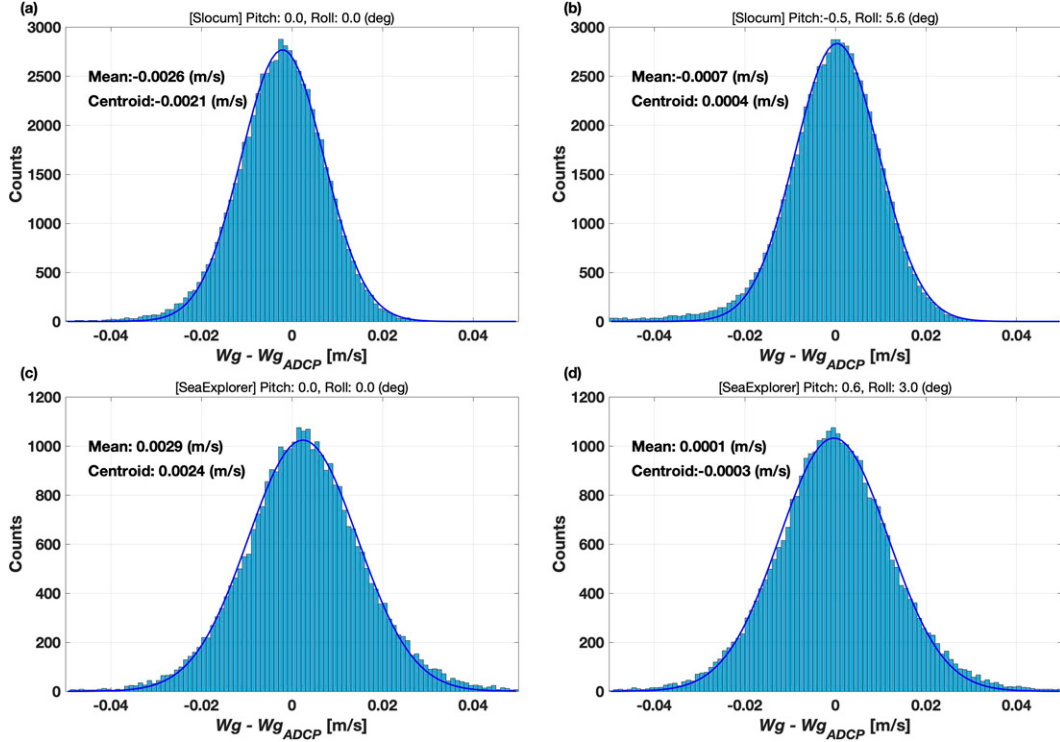


FIG. B1. (a) The histogram of the difference in  $w_g$  derived from the ADCP and the navigation depth sensor at each data point for the Slocum mission. A blue curve is the Gaussian function fitted to the histogram whose centroid value is shown in the panel. (b) As in (a), but after the offset of pitch and roll angle in the title was corrected. (c),(d) As in (a) and (b), but for SeaExplorer mission.

Figures C1a–c are the time series of echo intensity, percent good, and SNR for all the bins during the whole Slocum glider mission. The echo intensity was about 40 at the nearest bin but dropped very rapidly to the noise level (26.5 dB) at deeper bins due to the low input voltage of our ADCP and/or insufficient backscatters in the seawater (Fig. C1a). As a result, SNR typically exceeded 20 (i.e., the initial QC criteria R4 in section 2b) only at the nearest bin (Fig. C1c), although the percent good was 100 down to around bin5 (Fig. C1b). Since almost all of the data at deeper bins did not pass R4, the analysis for the deeper bins relaxed this criterion to  $\text{SNR} > 3$  following MEA19. For Nortek ADCP of the SeaExplorer, on the other hand, the echo intensity, or amplitude, was still as high as 40 dB down to about bin5 (Fig. C1d). SNR was thus higher than 20 down to bin5 as well (Fig. C1f), and the correlation was also higher than 50 down to bin10 (Fig. C1e). So the initial data QC criteria for deeper bins were the same as for the nearest bin for the Nortek ADCP.

The mean  $u_p$ ,  $v_p$ , and  $w_p$  at each bin with 95% confidence interval ( $=1.96 \times \text{standard error}$ ) was calculated from Eqs. (12)–(14) before going through the initial QC (Figs. C1g–i,j–l for the whole Slocum and SeaExplorer glider mission, respectively). The mean velocity at the nearest bin deviated from those at the rest of the bins as mentioned by MEA19 for the Slocum glider (Figs. C1g–i).  $w_p$  at the nearest bin was about 5% and 10% larger than

that at bin2 and bin3–6, respectively (Fig. C1i). This larger  $w_p$  at bin1 was also seen even after passing the initial QC.

After selecting the data based on section 2b, the lift and drag coefficients were estimated by the regression method of this study (section 3a) using velocity at bin1–bin4 of the Slocum glider (Fig. C2a). The modeled AOAs with the resultant coefficients estimated from bin1 and bin2 velocity were about 0.2° larger than those at bin3 and bin4 due to larger  $w_p$  of bin1 and bin2. To confirm whether the obtained lift and drag coefficients satisfied the horizontal and vertical constraints of the glider motion, the modified MEA19 method was applied following section 4b. Although the resultant  $C_{D0}$  did not differ by more than 5% from the results of regression analysis for all bins, the total lift coefficient,  $a$ , got increased by about 10% for bin3 and bin4. Also, CF2 values of bin3 and bin4 became larger than bin1 and bin2 (Fig. C2b). Regarding the SeaExplorer, the modeled AOAs from bin1–bin4 agreed at the 5% level (i.e., 0.25°) for the nominal pitch angle of 20°–30° (Fig. C2c). The obtained  $C_{D0}$  and  $a$  did not differ by more than 5% from those obtained by the modified MEA19 method for all of the bins (Fig. C2d).

These results suggest that if the initial data QC of TEA17 is met, the lift and drag coefficients estimated by our regression method also satisfies the vertical and horizontal constraints of the glider motion, and the resultant

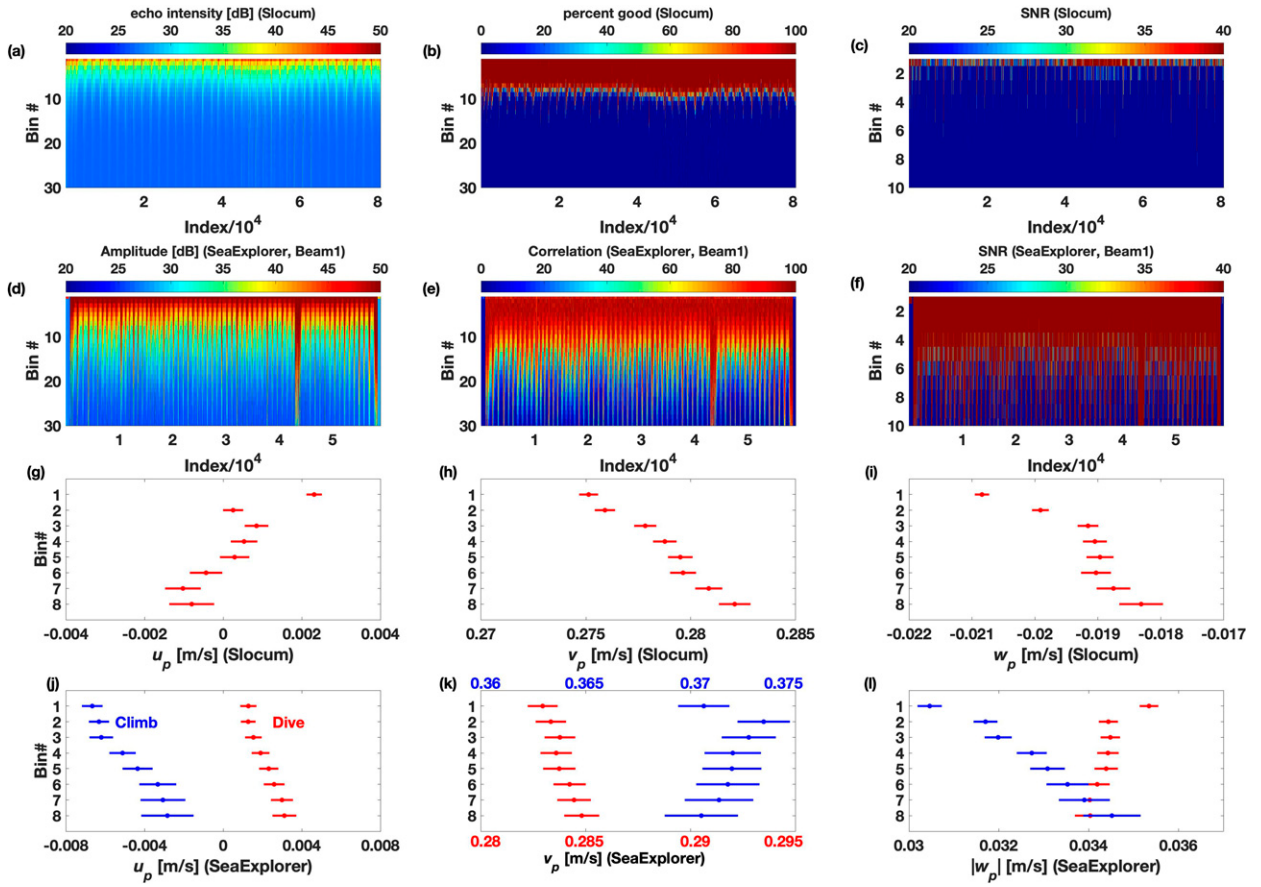


FIG. C1. The (a) echo intensity, (b) percent good, and (c) signal-to-noise ratio (SNR) at each bin of the ADCP during the whole Slocum mission. The (d) amplitude, (e) correlation, and (f) SNR for the whole SeaExplorer mission. The mean (g) cross-, (h) along-, and (i) vertical-glider velocities at each bin for the whole Slocum mission. Bars are the 95% confidence intervals computed by the mean  $\pm 1.96 \times$  standard error. (j)–(l) As in (g)–(i), but for the SeaExplorer mission.

modeled AOA agrees within a factor of 5% between bins. We note that the minimum CF2 values of the SeaExplorer mission were smaller for bin2 and bin3 than for bin1 (Fig. C2d). This might be because the bin1 velocity during ascent was affected by the flow distortion induced by the glider's body. Atmospheric observations by ultrasonic anemometers reported underestimation of vertical velocity due to the flow distortion by the frame of anemometer under laminar (e.g., van der Molen et al. 2004; Nakai et al. 2006) as well as turbulent conditions (e.g., Nakai and Shimoyama 2012). Since the acoustic gliders and anemometers are completely different platforms (i.e., the glider is a moving platform where the nearest bin is about 1 m or more away from the transducer, while the anemometer is a platform fixed to the ground, and the wind velocity measurement is made only 0.1–0.2 m apart from the transducer), further studies and observational data are necessary to assess whether the similar influence of flow distortion also takes place in the glider observation. We also note that the bin mapping used for our RDI ADCP might affect the velocity measurements at deeper bins and increase the uncertainty in estimating the lift and drag coefficients. To

avoid this influence, the use of beam coordinate should be recommended for further studies on the glider flight modeling as we used for the SeaExplorer mission.

## APPENDIX D

### The Influence of Spikes on the Estimation of Lift and Drag Coefficients

To remove spikes seen in the velocity measurements, a median filter was applied to the raw velocity data prior to the data processing described in section 2. In this study, the spikes were detected if the deviation from the median value of each 40 (20) data points segment exceeded 1.5 times the standard deviation of the segment for the Slocum (SeaExplorer) glider mission using the median\_filter.m code in ODAS MATLAB Library (version 4.4 from Rockland Scientific Inc.). Figures D1b and D1d are examples of raw and filtered velocity time series for a cast of Slocum and SeaExplorer mission down to 1000 and 700 m (Figs. D1a,c), respectively, to show how this median filter

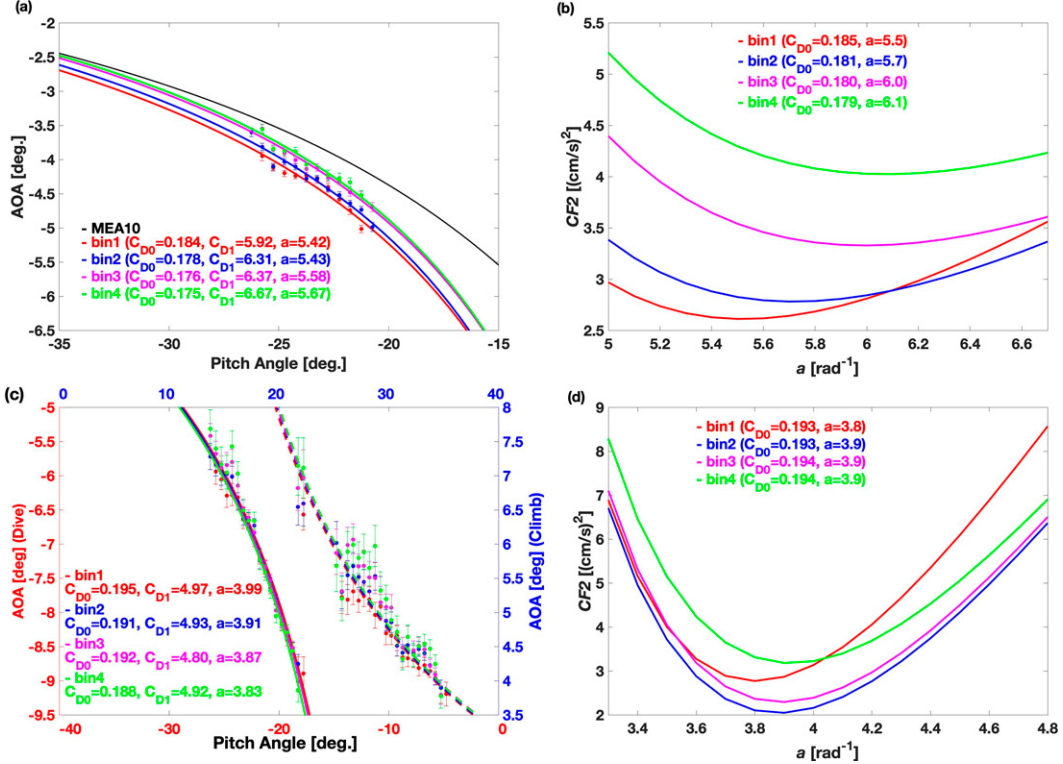


FIG. C2. (a) Dots are the observed pitch–AOA relationship averaged in each  $0.5^\circ$  pitch bin based on the velocity measurements at bin1–bin4 of the Slocum ADCP. An error bar denotes 95% confidence interval at each pitch bin estimated by the bootstrap method (Efron and Gong, 1983). Colored solid lines are the modeled AOA using the drag and lift coefficients derived from the bin1–bin4 velocity data. A black curve is the modeled AOA using the drag and lift coefficients of MEA10. (b) The variation of  $C_{D0}$  and CF2 with respect to the total lift coefficient  $a$  obtained by the modified MEA19 method using velocity data at each bin of the Slocum ADCP. (c),(d) As in (a) and (b), respectively, but for the SeaExplorer mission. Note that in (c), the y axis of the descent cast is on the left, while the ascent one is on the right. Solid and dashed lines in (c) are the modeled AOA for the descent and ascent, respectively.

worked to remove obvious large spikes. Using the filtered velocity data, the lift and drag coefficients were estimated by the same regression method as used for the raw velocity data. The modeled AOA with the coefficients derived from the filtered velocity did not differ by more than  $0.1^\circ$  for the nominal pitch angle of  $20^\circ$ – $30^\circ$  for both gliders (Figs. D1e,f) suggesting that the data selection procedure in section 3 reduced the influence of spikes on estimating the lift and drag coefficients.

## APPENDIX E

### AOA Derived from EM Sensor

The EM sensor is another source of velocity measurement and can be used to yield AOA as follows. Based on  $v_p$  and  $w_g$ , measured by the EM and the pressure sensor, respectively. The geometry in Fig. 1a gives

$$v_g \sin(\theta + \alpha) = w_g, \quad (\text{E1})$$

$$v_p = v_g \cos\alpha, \quad (\text{E2})$$

and then the AOA can be calculated as

$$\alpha = \arctan \left( \frac{w_g}{v_p \cos\theta} - \tan \theta \right). \quad (\text{E3})$$

Since MEA19 reported that  $v_p$  measured by the EM sensor was overestimated for unknown reasons, we compared  $v_p$  obtained simultaneously by the EM sensor and ADCP. The histograms of  $v_p_{\text{ADCP}}/v_p_{\text{EM}}$  were well fit by a Gaussian distribution that had peaks at 0.85 and 0.90 for the Slocum and SeaExplorer, respectively, indicating our EM sensors were also overestimating  $v_p$  (Figs. E1a,b). Applying these scaling factors to our EM sensor data, the resultant pitch–AOA relationship had a fair agreement with that derived from AOA estimated by the ADCP (black dots in Figs. 4f, 6c,d).

As we mentioned in section 3a, MEA19's lift and drag coefficients would not give a closer agreement between the modeled AOA and the AOA estimated by our ADCP data (Fig. 4f). If the scaling factor is determined in the same way as MEA19 described (i.e., by achieving  $\sin(\theta + \alpha)/\cos(\alpha) = w_g/v_p_{\text{EM}}$ , where  $\alpha$  is the modeled AOA using MEA19's coefficients, and the offset of  $\theta$  is corrected), the resultant scaling factor would be 0.90 based on the descent casts we analyzed (Fig. E1c). Using this scaling factor, the AOA estimated by the EM

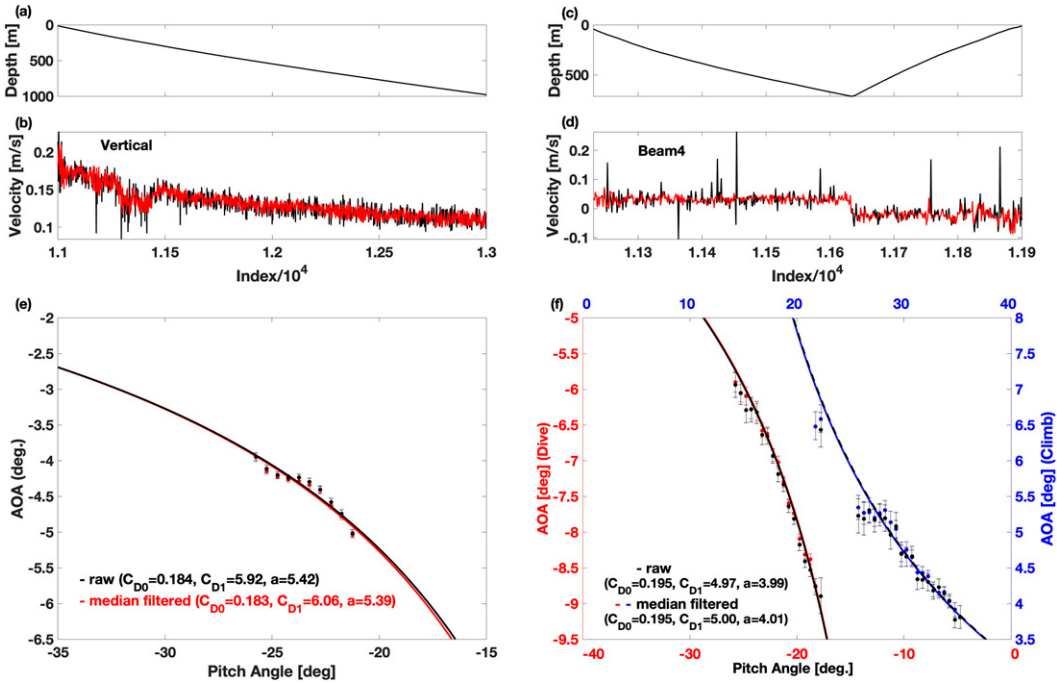


FIG. D1. The (a) depth and (b) vertical velocity recorded by the Slocum ADCP during a cast down to 1000 m. The red line in (b) is median filtered. (c),(d) As in (a) and (b), but for beam4 velocity of the SeaExplorer. (e) Red (black) dots are the observed pitch–AOA relationship averaged in each 0.5° pitch bin using the median filtered (raw) velocity data. An error bar denotes 95% confidence interval at each pitch bin estimated by the bootstrap method (Efron and Gong 1983). Red (black) solid lines are the modeled AOA using the drag and lift coefficients derived from the median filtered (raw) velocity data of the Slocum ADCP. The black dots and line are the same as green dots and a red line, respectively, in Fig. 4f. (f) As in (e), but for the SeaExplorer mission. Note that the red and blue line is for the descent and ascent, whose y axis is on the left and right, respectively.

sensor (blue dots in Fig. 4f) are well modeled with MEA19's coefficients (black dashed line in Fig. 4f), indicating that AOA estimation is highly sensitive to the scaling factor.

Since the MR provides the pressure, pitch, and  $v_p$  time series, it is natural to think that both the lift and drag coefficients can be estimated solely from the MR by the modified MEA19 method. The technical problem of using the MR data only is that the estimation of scaling factor needs the calculation of AOA. We have tested the following procedures to determine the lift and drag coefficients:

- EM1) Set an initial lift coefficient  $a$ .
- EM2) Compute  $C_{D0}$  (and  $V_g$  and  $c$ ) by the MEA10 method.
- EM3) Use AOA from the flight model to compute the proper scaling factor for the EM sensor from matching  $\sin(\theta + \alpha)/\cos(\alpha) = w_g/v_{p,EM}$ .
- EM4) Compute a new  $C_{D0}$  and  $a$  by the modified MEA19 method.
- EM5) Repeat from EM3 until the fractional change in  $C_{D0}$ ,  $a$ , and scaling factor between iterations are all less than 5%.

Based on our results from section 3,  $C_{D1}$  was set to be 5.9 and 5.0 rad<sup>-2</sup> for the Slocum and SeaExplorer, respectively. As for the Slocum, Figs. E1d and E1e are the results

of EM3 and EM4, respectively, for the first iteration when the initial lift coefficient was set to be 4.8 rad<sup>-1</sup>, showing that the newly obtained  $C_{D0}$  and  $a$  (=0.19 and 4.9 rad<sup>-1</sup>, respectively) changed less than 5% of those initially set in EM1 and EM2. This indicates that the final lift and drag coefficients were strongly dependent on the initial lift coefficient set in EM1, which was true for other initial values examined ( $a = 4.8\text{--}6.0 \text{ rad}^{-1}$ ) and also true for the SeaExplorer case. This is because adjusting the scaling factor in EM3 minimized the difference between the modeled and measured axial speed of the glider for the lift coefficient initially set in EM1. These results indicate that the optimum set of lift and drag coefficients and scaling factor cannot be determined uniquely without having another source of velocity measurement.

We would like to note that the scaling factor of 0.85 for the Slocum does not necessarily work best for all the individual casts during the mission. Also, our MR data showed that the scaling factor for ascent (~0.91) was different from that for descent (~0.85). The reasons for this discrepancy between the descent and ascent have not been identified yet although the disturbance from the MR/glider body under different descent/ascent flight conditions and the additional influence of AOA to the velocity measurement of EM sensor might possibly be involved. Calibration of EM sensors in a tow tank while keeping the EM sensor attached

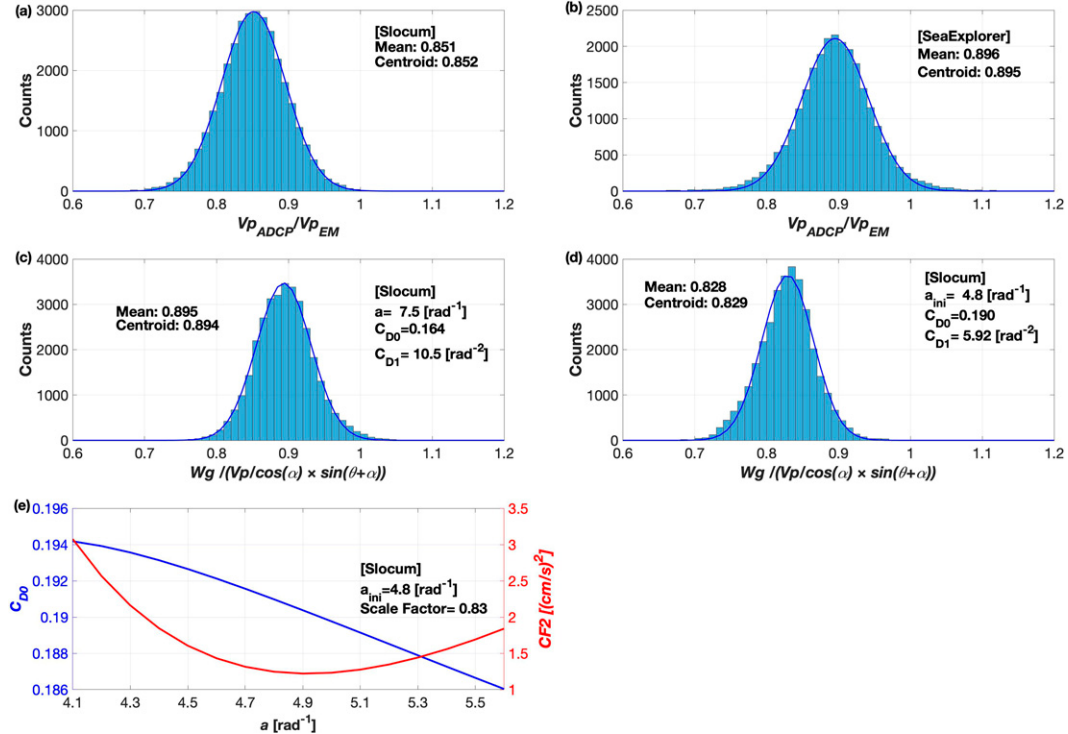


FIG. E1. (a) The histogram of the ratio of  $v_p$  derived from the ADCP to that from the EM sensor for the Slocum mission. The blue curve is the Gaussian function fitted to the histogram whose centroid value is shown in the panel. (b) As in (a), but for the SeaExplorer mission. (c) A histogram of the ratio of  $w_g$  derived from the CTD depth sensor to that derived from  $v_p$  measured by the EM sensor and the modeled AOA for the Slocum mission. Modeled AOA was calculated based on the lift and drag coefficients of MEA19. (d) As in (c), but using the modeled AOA calculated based on the lift and drag coefficients determined by the method described in section 4b. (e) The variation of  $C_{D0}$  and  $CF2$  with respect to the total lift coefficient,  $a$ , obtained by the modified MEA19 method using the EM sensor whose scale factor was set to 0.83.

to the MR/glider should be done in the future to determine a proper method to correct the EM sensor data.

## REFERENCES

- Bennett, J. S., F. R. Stahr, C. C. Eriksen, M. C. Renken, W. E. Snyder, and L. J. Van Uffelen, 2021: Assessing Seaglider model-based position accuracy on an acoustic tracking range. *J. Atmos. Oceanic Technol.*, **38**, 1111–1123, <https://doi.org/10.1175/JTECH-D-20-0091.1>.
- Cooney, L., 2011: Angle of attack and Slocum vehicle model. Teledyne Webb Research Tech. Rep., 7 pp.
- de Fommervault, O., F. Besson, L. Beguery, Y. Le Page, and P. Llettes, 2019: SeaExplorer underwater glider: A new tool to measure depth-resolved water currents profiles. *OCEANS 2019*, Marseille, France, IEEE, <https://doi.org/10.1109/OCEANSE.2019.8867228>.
- Deines, K. L., 1999: Backscatter estimation using broadband acoustic Doppler current profilers. *Proc. Sixth Working Conf. on Current Measurement*, San Diego, CA, IEEE, 249–253, <https://doi.org/10.1109/CCM.1999.755249>.
- Efron, B., and G. Gong, 1983: A leisurely look at the bootstrap, the jackknife, and cross-validation. *Amer. Stat.*, **37**, 36–48, <https://doi.org/10.2307/2685844>.
- Fer, I., A. K. Peterson, and J. E. Ullgren, 2014: Microstructure measurements from an underwater glider in the turbulent Faroe Bank Channel overflow. *J. Atmos. Oceanic Technol.*, **31**, 1128–1150, <https://doi.org/10.1175/JTECH-D-13-00221.1>.
- Frajka-Williams, E., C. C. Eriksen, P. B. Rhines, and R. R. Harcourt, 2011: Determining vertical water velocities from Seaglider. *J. Atmos. Oceanic Technol.*, **28**, 1641–1656, <https://doi.org/10.1175/2011JTECHO830.1>.
- Garau, B., S. Ruiz, W. G. Zhang, A. Pascual, E. Heslop, J. Kerfoot, and J. Tintoré, 2011: Thermal lag correction on Slocum CTD glider data. *J. Atmos. Oceanic Technol.*, **28**, 1065–1071, <https://doi.org/10.1175/JTECH-D-10-05030.1>.
- Lueck, R. G., D. Huang, D. Newman, and J. Box, 1997: Turbulence measurement with a moored instrument. *J. Atmos. Oceanic Technol.*, **14**, 143–161, [https://doi.org/10.1175/1520-0426\(1997\)014<0143:TMWAMI>2.0.CO;2](https://doi.org/10.1175/1520-0426(1997)014<0143:TMWAMI>2.0.CO;2).
- Merkelbach, L., D. Smeed, and G. Griffiths, 2010: Vertical velocities from underwater gliders. *J. Atmos. Oceanic Technol.*, **27**, 547–563, <https://doi.org/10.1175/2009JTECHO710.1>.
- , A. Berger, G. Krahmann, M. Dengler, and J. R. Carpenter, 2019: A dynamic flight model for Slocum gliders and implications for turbulence microstructure measurements. *J. Atmos. Oceanic Technol.*, **36**, 281–296, <https://doi.org/10.1175/JTECH-D-18-0168.1>.

- Munk, W. H., and A. M. G. Forbes, 1989: Global ocean warming: An acoustic measure? *J. Phys. Oceanogr.*, **19**, 1765–1778, [https://doi.org/10.1175/1520-0485\(1989\)019<1765:GOWAAM>2.0.CO;2](https://doi.org/10.1175/1520-0485(1989)019<1765:GOWAAM>2.0.CO;2).
- Nakai, T., and K. Shimoyama, 2012: Ultrasonic anemometer angle of attack errors under turbulent conditions. *Agric. For. Meteor.*, **162–163**, 14–26, <https://doi.org/10.1016/j.agrformet.2012.04.004>.
- , M. K. van der Molen, J. H. C. Gash, and Y. Kodama, 2006: Correction of sonic anemometer angle of attack errors. *Agric. For. Meteor.*, **136**, 19–30, <https://doi.org/10.1016/j.agrformet.2006.01.006>.
- Osborn, T. R., 1974: Vertical profiling of velocity microstructure. *J. Phys. Oceanogr.*, **4**, 109–115, [https://doi.org/10.1175/1520-0485\(1974\)004<0109:VPOVM>2.0.CO;2](https://doi.org/10.1175/1520-0485(1974)004<0109:VPOVM>2.0.CO;2).
- Palmer, M., G. Stephenson, M. Inall, C. Balfour, A. Düsterhus, and J. A. M. Green, 2015: Turbulence and mixing by internal waves in the Celtic Sea determined from ocean glider microstructure measurements. *J. Mar. Syst.*, **144**, 57–69, <https://doi.org/10.1016/j.jmarsys.2014.11.005>.
- Peterson, A. K., and I. Fer, 2014: Dissipation measurements using temperature microstructure from an underwater glider. *Methods Oceanogr.*, **10**, 44–69, <https://doi.org/10.1016/j.mio.2014.05.002>.
- Rudnick, D., 2016: Ocean research enabled by underwater gliders. *Annu. Rev. Mar. Sci.*, **8**, 519–541, <https://doi.org/10.1146/annurev-marine-122414-033913>.
- , J. T. Sherman, and A. P. Wu, 2018: Depth-average velocity from Spray underwater gliders. *J. Atmos. Oceanic Technol.*, **35**, 1665–1673, <https://doi.org/10.1175/JTECH-D-17-0200.1>.
- Scheifele, B., S. Waterman, L. Merckelbach, and J. R. Carpenter, 2018: Measuring the dissipation rate of turbulent kinetic energy in strongly stratified, low-energy environments: A case study from the Arctic Ocean. *J. Geophys. Res. Oceans*, **123**, 5459–5480, <https://doi.org/10.1029/2017JC013731>.
- Schmitt, R. W., and R. A. Petitt, 2006: A fast response, stable CTD for gliders and AUVs. *Oceans 2006*, Boston, MA, IEEE, <https://doi.org/10.1109/OCEANS.2006.306907>.
- Schultze, L. K. P., L. M. Merckelbach, and J. R. Carpenter, 2017: Turbulence and mixing in a shallow stratified shelf sea from underwater gliders. *J. Geophys. Res. Oceans*, **122**, 9092–9109, <https://doi.org/10.1002/2017JC012872>.
- Sherman, J., R. Davis, W. Owens, and J. Valdes, 2001: The autonomous underwater glider “Spray.” *IEEE J. Oceanic Eng.*, **26**, 437–446, <https://doi.org/10.1109/48.972076>.
- Teledyne Webb Research, 2012: Slocum G2 glider maintenance manual. Teledyne Webb Research Doc. P/N 4344, rev. B, 132 pp.
- Todd, R. E., D. L. Rudnick, J. T. Sherman, W. B. Owens, and L. George, 2017: Absolute velocity estimates from autonomous underwater gliders equipped with Doppler current profilers. *J. Atmos. Oceanic Technol.*, **34**, 309–333, <https://doi.org/10.1175/JTECH-D-16-0156.1>.
- van der Molen, M. K., J. H. C. Gash, and J. A. Elbers, 2004: Sonic anemometer (co)sine response and flux measurement: II. The effect of introducing an angle of attack dependent calibration. *Agric. For. Meteor.*, **122**, 95–109, <https://doi.org/10.1016/j.agrformet.2003.09.003>.
- Williams, C. D., R. Bachmayer, and B. DeYoung, 2008: Progress in predicting the performance of ocean gliders from at-sea measurements. *OCEANS 2008*, Quebec City, QC, Canada, IEEE, <https://doi.org/10.1109/OCEANS.2008.5152068>.

Copyright of Journal of Atmospheric & Oceanic Technology is the property of American Meteorological Society and its content may not be copied or emailed to multiple sites or posted to a listserv without the copyright holder's express written permission. However, users may print, download, or email articles for individual use.